

Pro Gradu

**Dielectrophoresis as an assembly method for
carbon nanotube memory elements**



Tommi Isoniemi

April 24, 2010

UNIVERSITY OF JYVÄSKYLÄ
NANOSCIENCE CENTER
DEPARTMENT OF PHYSICS
NANOELECTRONICS

Preface

The experiments reviewed in this Master's thesis have been carried out at Nanoscience Center, Department of Physics in the University of Jyväskylä between January 2008 and December 2008.

I would like to thank my supervisors, Dr. Andreas Johansson and Dr. Marcus Rinkiö, for giving me an opportunity to work in the Nanoelectronics research group as well as providing practical guidance in experimental matters. I would also like to thank everyone, especially in the ELE group, who has supported me in the making of this thesis.

Jyväskylä April 24, 2010

Tommi Isoniemi

Abstract

The experiments described in this Master's thesis aim to assess the practicality of using dielectrophoresis (DEP) for assembling memory elements from carbon nanotubes (CNTs). These elements were field-effect transistors (FETs) with a wide hysteresis window.

The devices assessed were made on a silicon substrate with a HfO_2 - TiO_2 - HfO_2 gate dielectric layer to ensure a predictable hysteresis for memory operation. The FETs were used for further research in regard to environmental effects in their operation. [1]

An average yield of 12.5 % over 26 different trapping attempts, a total of 650 gaps, was achieved for single trapped CNTs in a two-electrode configuration with a 1 μm gap between electrodes with a width of 300 nm. The electrical parameters for DEP ($f = 300$ kHz, $V_{PP} = 5$ V, $t \approx 2$ min) were consistent in the batch, but the CNT mass concentration of the 1,2-dichloroethane suspension varied between 1/98000 and 1/270000. 47 successful FETs with hysteresis were produced in the 350 devices evaluated by electrical measurements.

Trapping the nanotubes exclusively on electrode tips was not possible with the configuration used in the experiments. Additionally, controlling the concentration of CNTs in the suspension was difficult. This resulted in unpredictable amounts of material between different samples as well as separate gaps between electrodes in the same sample. Because surfactants weren't used, the widespread attachment of the CNTs to each other also posed a problem.

The FET operation testing was hampered by current leaks through the gate dielectric. The devices that were produced also had a relatively high current in the off-state, which resulted in low on/off ratios for the CNTFETs.

Contents

Introduction	5
1 Carbon Nanotubes	6
1.1 Structure	6
1.1.1 Bundles and MWCNTs	7
1.2 Electronic properties	8
1.2.1 Graphene	8
1.2.2 The SWCNT as a one-dimensional structure	8
1.2.3 Conductance	12
1.3 Transconductance	13
1.3.1 Carbon nanotube field-effect transistor	15
1.3.2 CNTFET memory elements	16
2 Dielectrophoresis	19
2.1 Dielectrophoretic force	20
2.2 Dielectrophoretic potential	22
2.3 Electric fields in DEP	22
2.4 Brownian motion	22
2.5 Fluid dynamics	24
2.6 Applications	26
2.7 DEP on CNTs	28
3 Sample fabrication	30
3.1 Substrate	30
3.2 Electrode design	30
3.3 Electron beam lithography	30
4 CNT trapping	35
4.1 CNT preparation	35
4.2 Experiment setup	35

5	Results	37
5.1	CNT placement	37
5.1.1	Two-electrode configuration	37
5.1.2	Four-electrode configuration	39
5.2	FET measurements	39
5.2.1	Effect of an extra Pd layer	44
6	Conclusions	50
6.1	CNT trapping	50
6.2	FET operation	51

Introduction

Carbon-based structures show much potential in nanoelectronics. Carbon nanotubes have been envisioned to enable further miniaturization in electronic components and circuits due to their promising electronic properties and durability. In particular, the high current density possible in metallic tubes and transconductance properties of semiconducting tubes are promising for applications.

Dielectrophoresis is a technique that can be used to manipulate different polarizable particles with great selectivity. Non-uniform electric fields are used to induce a nonequal charge distribution in particles and to exert forces on them. Applied to CNTs, DEP is useful for attracting the tubes in a suspension to electrodes, positioning them to desired positions in electric circuits. It has become a basic method for manipulating microscale objects. DEP is based on the force caused on any polarizable object, charged or neutral, by a nonuniform electric field.

CNTFETs have previously been made with a variety of methods, from growing CNTs from electrode tips to producing electrical connects with lithography after locating the CNTs manually. All these methods, including DEP, have at the moment a very poor yield in comparison to transistors made with conventional silicon technology employed in the semiconductor industry.

The experiments presented in this Master's thesis aim to assess the practical possibility for producing carbon nanotube-based field effect transistors with DEP. Locating the CNTs is done with SEM micrographs and the transistor behaviour is quantified with electrical measurements. This research work was a part of the Tekes FinNano programme "Molecular Scale Memory Elements" and received support also from companies Nokia Oyj, Beneq Oy (previously Planar Inc.) and Vaisala Oyj.

The experimental results produced are presented in Chapter 5. Methods relating to sample fabrication and dielectrophoresis are described in Chapters 3 and 4. The first two Chapters include properties of carbon nanotubes and CNTFETs as well as material on dielectrophoresis. Conclusions about the work are discussed in the final chapter.

Chapter 1

Carbon Nanotubes

Carbon nanotubes are carbon molecules that can be viewed as rolled-up graphene strips which form closed cylinders, or alternatively as elongated fullerenes. Each carbon atom in a CNT has covalent bonds with three neighbors as in graphite, in contrast to diamond, another allotrope of carbon in which covalent bonds extend to four neighbors. The simplest tubes have only a single wall, but the first nanotubes characterized were made of several concentric shells with a regular spacing of 3.4 Å, i.e. multiwalled nanotubes. [2]

These molecular systems are nanometer-sized in diameter, but up to centimeters long. The high regularity of the molecular structure of CNTs as well as their similarity to graphene results in chemical inertness.

Like graphene under tension, CNTs are two orders of magnitude stronger than steel at one sixth of the mass. The theoretical Young's modulus of CNT bundles exceeds 1 TPa. The graphitic sp^2 bond is 33 % stronger than the sp^3 bond in diamond, which accounts for the high strength of the CNT in the direction of the tube axis. [3]

CNTs also remain stable up to very high temperatures, close to the melting point of graphite near 4000 K and their thermal conductivity along the tube axis is the highest of all materials. These properties are also due to the long structure being connected with strong covalent bonds. [3]

Synthesis methods for carbon nanotubes include arc-discharge, laser ablation, gas-phase catalytic growth from carbon monoxide and chemical vapor deposition (CVD) from hydrocarbons. The synthesis usually produces impurities in the form of catalyst particles, amorphous carbon and non-tubular fullerenes, which have to be removed by subsequent purification steps. [4] Producing primarily MWCNTs by milling graphite with steel balls and annealing the carbon product is also possible. [5]

1.1 Structure

The straight sections of CNTs have a regular hexagonal structure, but additional curvature can be created by defects that have pentagons or heptagons in them. In these

defects each carbon atom is still primarily bonded to its three nearest neighbors and there are no dangling bonds. The ends of CNTs as well as junctions and transitions between different chiralities are created by these defects (Fig. 1.1).

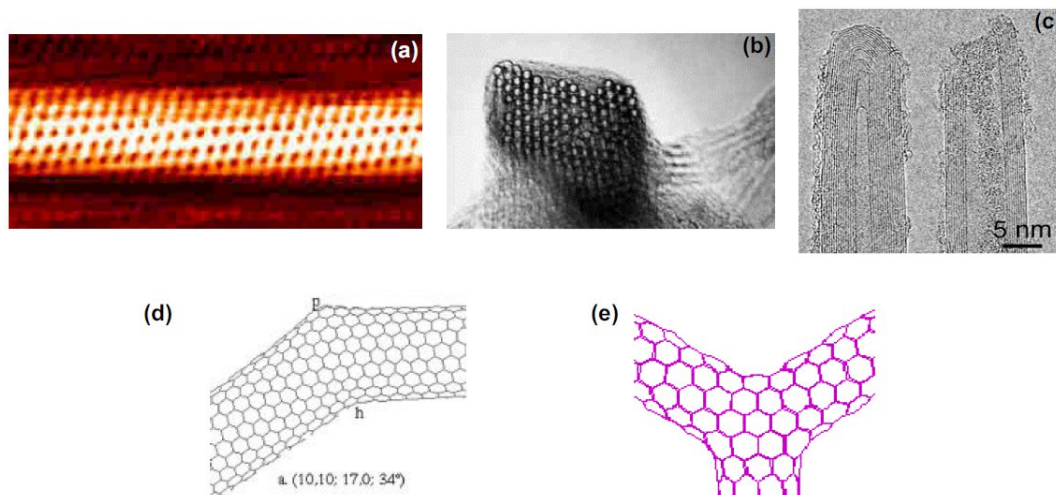


Figure 1.1: Different types of CNTs. (a) STM image of a SWCNT, (b) a SWCNT bundle, (c) two MWCNTs, (d) a junction between nanotubes of differing chiralities, (e) a three-terminal junction between nanotubes. Images published in [2].

1.1.1 Bundles and MWCNTs

Single-walled CNTs have a tendency to bundle due to van der Waals interactions. [4] Typical distances between tubes in bundles are similar to the interplanar distance in graphite (3.1 \AA). The cross section of an individual CNT in a bundle is circular if the diameter of the tube is less than 15 \AA and deforms to a hexagon for thicker tubes, maximising the contact area between the planes. [2]

Surfactants are commonly used to keep the tubes separate in suspensions. When using a polar liquid medium, these surfactants are usually long molecules with a polar (hydrophilic) and non-polar (hydrophobic) end. The non-polar end of the molecule sticks to the CNT and the polar end attracts molecules of the solvent.

Commonly used surfactants in aqueous solutions include two different families of encapsulating agents. The first group includes anionic-alkyl amphiphiles such as sodium dodecyl sulfate (SDS) and sodium dodecylbenzene sulphonate (SDBS), which have anionic head groups and flexible alkyl tails. The other group, bile salts like sodium cholate (SC) and sodium taurodeoxycholate, are more molecularly rigid and planar amphiphiles with a charged face opposing a hydrophobic one. [6]

The close proximity of CNTs in bundles affects the electrical properties of single tubes. For example, armchair tubes ($n = m$) with metallic properties individually can have significant bandgaps (0.1 eV for $(10,10)$ CNTs) when bundled. [7] Individual

tubes in bundles as well as concentric shells in multiwall CNTs can also transfer charge to each other through π bonds.

1.2 Electronic properties

Experiments and theory have shown that single-walled carbon nanotubes can be either metallic or semiconducting. These properties stem from the electronic structure of graphene, a two-dimensional structure of sp^2 bonded carbon atoms. The hexagonal structure of graphene provides a good starting point for understanding the electronic properties of CNTs. [8]

1.2.1 Graphene

In the graphene sheet σ bonds are formed by three out of four valence electrons along the surface of the sheet. [9] The remaining single valence electron per carbon atom forms π bonds that are perpendicular to the surface of the sheet by hybridization with first neighbors. [10] These bonds are illustrated in Fig. 1.2 with their energy bands.

The σ bonds are strong covalent bonds providing most of the binding energy and elastic properties of the graphene sheet. The energy levels associated with these bonds are far away from the Fermi energy in graphite and thus do not play a key role in its electronic properties. [11]

The π bonds are responsible for the conduction through the sheet as their energy bands cross the Fermi level at high-symmetry points in the Brillouin zone of graphene (Fig. 1.2). Additionally the π bonds determine the weak interaction between SWCNTs in a bundle in a similar way as different layers in graphite bond together.

The graphene structure has conducting states at the Fermi energy E_F , but only at specific points along certain directions in momentum space at the corners of the first Brillouin zone (Fig. 1.3 (b)). For this reason graphene is a semimetal: the structure is metallic in some directions and semiconducting in others. [11]

1.2.2 The SWCNT as a one-dimensional structure

As the structure of a SWCNT is a rolled-up graphene sheet, the momentum of the electrons around the circumference of the tube is quantized. This reduces the available states to slices through the 2D band structure and as such the tubes are either one-dimensional metals or semiconductors. If the tube axis points to a metallic direction on the graphene sheet, the tube acts as a 1D metal. [8]

The tube orientation on the graphene sheet is defined by the chiral vector [12]

$$\vec{C} = n\vec{a}_1 + m\vec{a}_2 \quad (1.1)$$

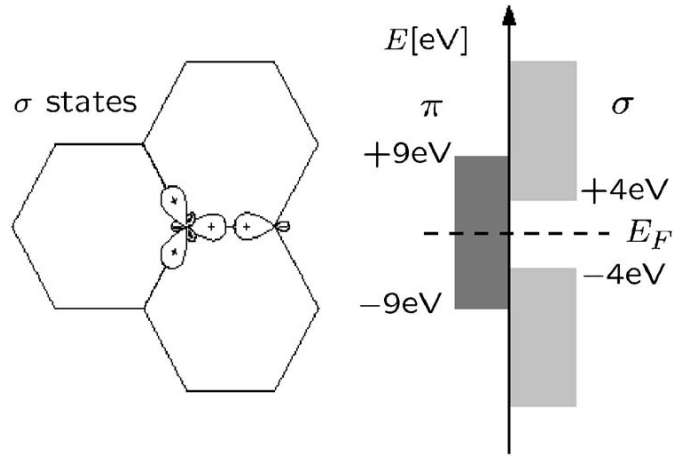


Figure 1.2: The bonds in a hexagonal carbon network. σ bonds connect the carbon atoms and are responsible for the strength and the elastic properties of the graphene sheet. The bonding and antibonding σ states are separated by a large energy gap. The π bonds are perpendicular to the sheet and their states lie in the vicinity of the Fermi level E_F . From [11].

where n and m are integers. \vec{a}_1 and \vec{a}_2 are the unit cell vectors of the 2D graphene lattice as in Fig. 1.5. The length of the chiral vector is the circumference c of the nanotube

$$c = |\vec{C}| = a\sqrt{n^2 + nm + m^2} \quad (1.2)$$

where a is the length of the unit cell vectors and it is related to the carbon-carbon bond length with $a = a_{cc}\sqrt{3}$. The bond length $a_{cc} = 0.1421$ nm for graphite, but the curvature of the nanotube results in the approximation $a_{cc} = 0.144$ nm for CNTs. The chiral vector can be determined as in Fig. 1.4. The chiral angle θ in the figure is defined as the angle between the chiral vector and \vec{a}_1 (the zig-zag direction of the graphene sheet) and can be calculated with [11]

$$\tan \theta = \frac{\sqrt{3}m}{2n + m}. \quad (1.3)$$

The magnitude of the energy gap in single-walled nanotubes varies with the direction of the chiral vector and as such the integers m and n . If $n - m$ is either zero or divisible by three, the SWCNT is metallic (band gap either zero or very small), otherwise it is semiconducting (Fig. 1.5). This result follows from a zone folding approximation. In reality also $(n,0)$ zig-zag tubes with n as a multiple of 3 have a small band gap and are semiconducting. [10] In some sources only tubes with $n = m$ (band

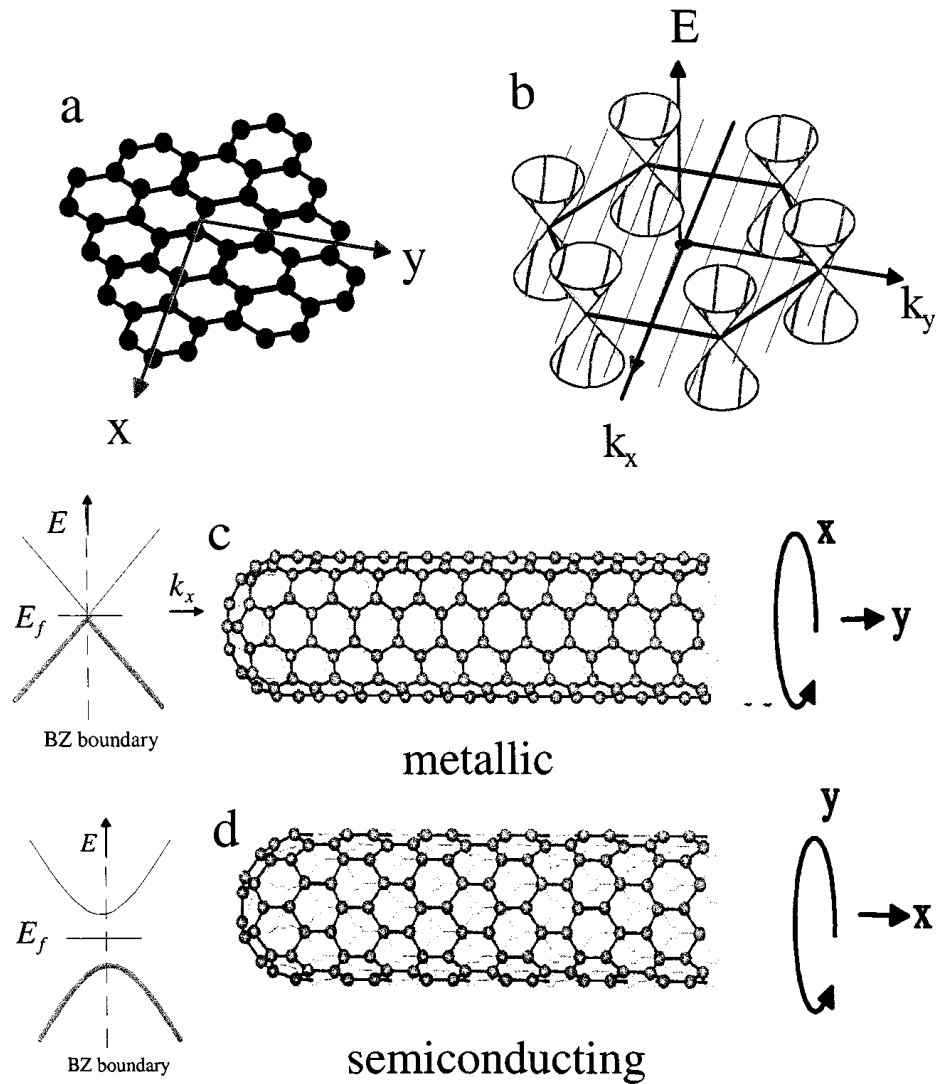


Figure 1.3: (a) The lattice structure of graphene. (b) Energy of the conducting states as a function of the electron wavevector k . (c), (d) Carbon nanotubes with their respective energy gaps shown at the Brillouin zone boundary. Illustrations from [8].

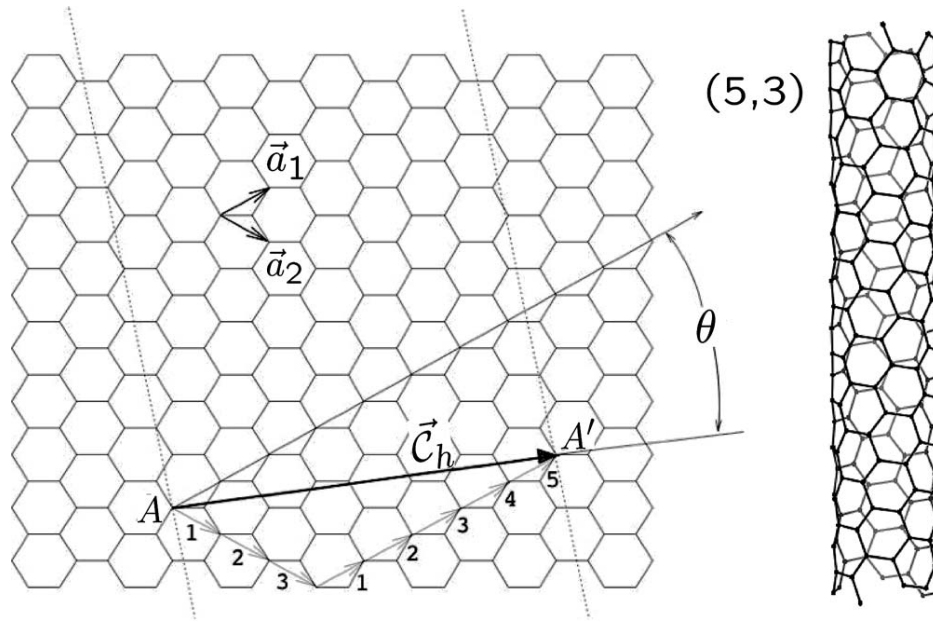


Figure 1.4: An example of the determination of a chiral vector for a (5,3) nanotube. The end points A and A' of the chiral vector are the same point in the SWCNT. From [11].

gap 0 eV without curvature effects) are referred to as metallic and the other tubes satisfying the condition mentioned before are considered semimetallic. [11]

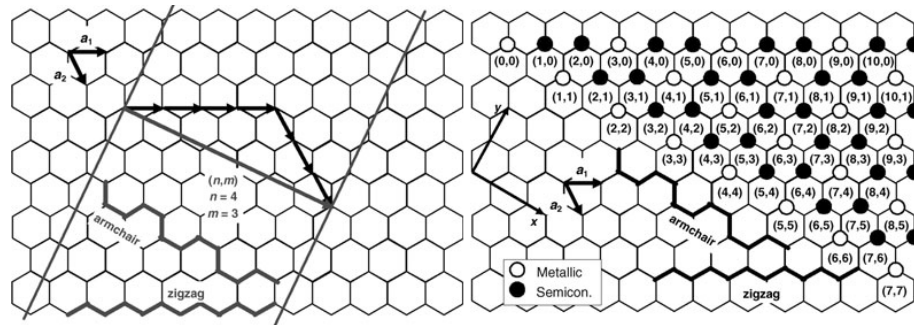


Figure 1.5: The definition of the chiral vector (n,m) in a SWCNT (left). Electrical properties of tubes with different chiralities (right). From [13].

Figure 1.6 shows the calculated density of states of a semiconducting and a metallic SWCNT. The semiconducting tube has an energy gap at E_F while the metallic one has a continuum of energy states at the Fermi level.

In the zone folding approximation, which approximates a CNT as a flat stripe of graphene, the π orbitals and the σ states are strictly perpendicular to each other and cannot mix. The curvature of CNTs, however, means that these states mix and form

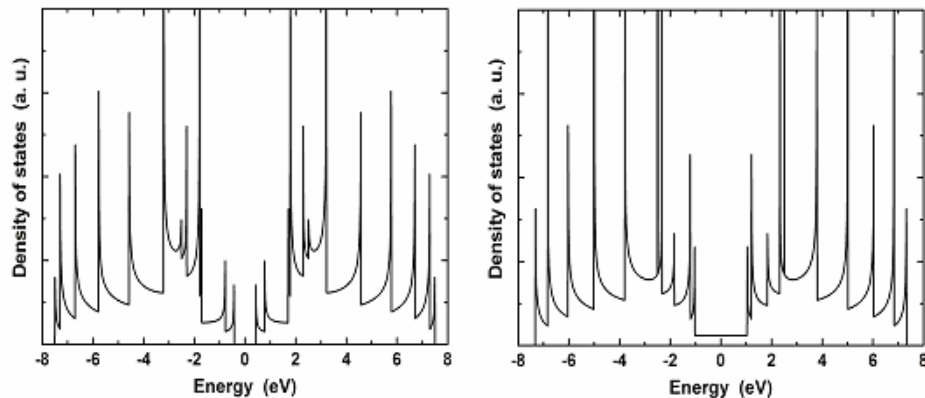


Figure 1.6: Density of states from tight binding calculations done in [2] for (11,0) (left) and (12,0) (right) CNTs. (11,0) is a semiconducting tube with no states around E_F and (12,0) a metallic tube with a non-zero DOS at the Fermi energy. Van Hove singularities, indicative of quasi-one-dimensional materials, are seen.

hybrids that are partly sp^2 and partly sp^3 in character. [14]

With curvature effects the π -derived bands (near the Fermi energy) in zig-zag ($m = 0$) and small chiral angle θ SWCNTs are strongly shifted to lower energy. Armchair and large θ tubes are weakly affected. [14]

1.2.3 Conductance

A metallic CNT can be considered a ballistic conductor, i.e. electrons are not scattered in a conductor, which is connected to two electrodes. [3] The electrodes have two different energy levels E_{F_1} and E_{F_2} ($E_{F_1} > E_{F_2}$). The resistance of such a ballistic conductor is given by

$$R_c = \frac{E_{F_1} - E_{F_2}}{eI} = \frac{h}{2e^2M}, \quad (1.4)$$

where R_c is the contact resistance, I the current through the conductor, h Planck constant, e elementary charge, $\frac{h}{2e^2} \approx 12.9 \text{ k}\Omega$ the quantized resistance R_0 and M the number of conduction channels. [15] This means that the nanotube conductance is quantized in multiples of the fundamental conductance quantum $G_0 = \frac{1}{R_0}$.

This quantum-mechanical contact resistance arises from the mismatch of the numbers of conduction channels in the mesoscopic conductor and the macroscopic metal connector. Poor coupling between the metal leads and the CNT can contribute additional contact resistance. [15]

The length over which a CNT can behave as a ballistic conductor depends on its structural perfection, temperature and the size of the driving electric field. In general, ballistic transport can be achieved over lengths typical of modern scaled electronic

devices (≤ 100 nm). [16] If the electrons scatter in the conductor, the transport is diffusive and with a large number of scattering events an ohmic response will be observed as in conventional conductors. The quasi-ballistic transport in CNTs means that a CNTFET with a channel length of 50 nm has essentially the same electrical behaviour than one with a 300 nm channel length. [17]

In a SWCNT with a diameter of 1 – 2 nm the number of conduction channels M is one when the bias voltage $E_{F_1} - E_{F_2} < 1$ eV. A metallic armchair (zig-zag) tube close to the Fermi energy has doubly degenerate ($M = 2$) bands so the total quantum conductance is [9]

$$G_Q = 2G_0 = \frac{4e^2}{h}. \quad (1.5)$$

Independent of the conduction type and intrinsic to nanotubes, it is the nature of the contact that ultimately determines their conductance behaviour in a circuit. [3] Metals with a work function sufficiently greater or smaller than that of a nanotube will form ohmic contacts with the nanotube. A Schottky barrier will be formed if the metal work function is on a similar level. [1]

1.3 Transconductance

Whereas metallic, particularly multiwalled, CNTs can be used as high-performance interconnects in very-large-scale integrated systems, the current in semiconducting CNTs can be switched on or off. In general, this modulation in semiconductors can be done with some kind of activation, such as heating or light absorption, to get the charge carriers over the gap. The gap itself can be modulated by some external influence such as applied strain, magnetic field or electric field. [16]

If an external electric field is applied on a nanotube, the density of states of the system is changed due to the spontaneous breaking of symmetry of the quantum mechanical Hamiltonian. The most relevant effect for applications is the opening and closing of the band gap at Fermi level, which changes the conductance of the tube (Fig. 1.7). [18]

An example of the band structure changing in response to an external electric field is shown in Fig. 1.8. The metallic (10,10) SWCNT has the two lowest subbands always crossing, but the density of states increases near the Fermi level. The armchair ($n = m$) tubes remain metallic in strong uniform fields, but for other chiralities the band gap opens and closes for different field strengths as in Fig. 1.7. The electric field is assumed to be uniform at the size scale of the nanotube diameter in these simulations.

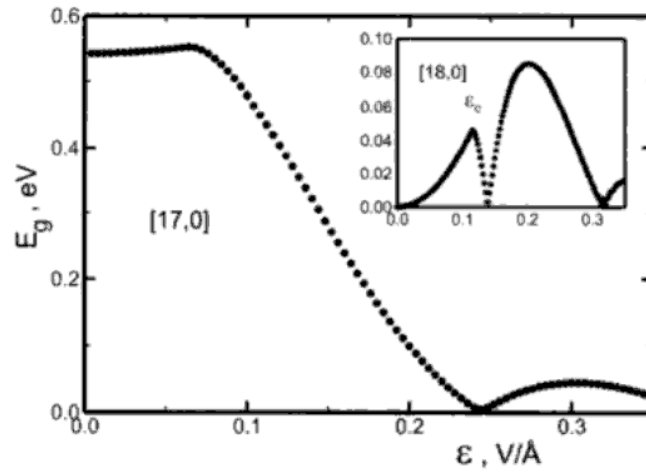


Figure 1.7: Band gap variation of SWCNTs as a function of electric field strength. Tubes simulated are (17,0) and (18,0) in inset. From [18].

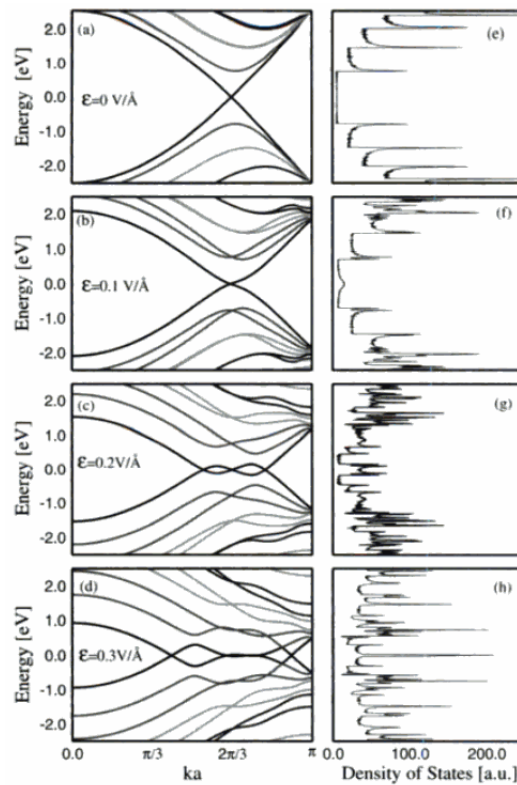


Figure 1.8: Band structure and density of states of a (10,10) armchair CNT at different perpendicular electric fields. Simulations from [18].

1.3.1 Carbon nanotube field-effect transistor

In a field-effect transistor (FET) a semiconducting channel is modulated by an electric field. The semiconductor is connected to two electrodes, source and drain, and the electric field controlling the electric current in the channel is produced by applying a voltage to a gate electrode. [1]

In a CNTFET (Fig. 1.9 a)) the semiconducting channel is composed of one or more carbon nanotubes. The behaviour in CNTFETs (Fig. 1.9 b)) resemble those of conventional p-type silicon MOSFETs, but it is not a result of a certain doping level in the nanotube. CNTFET operation is controlled by Schottky barriers in the interface between the source and drain electrodes and the nanotube rather than the nanotube itself. The existence of these barriers has been confirmed by means of local gating with an AFM tip. [19]

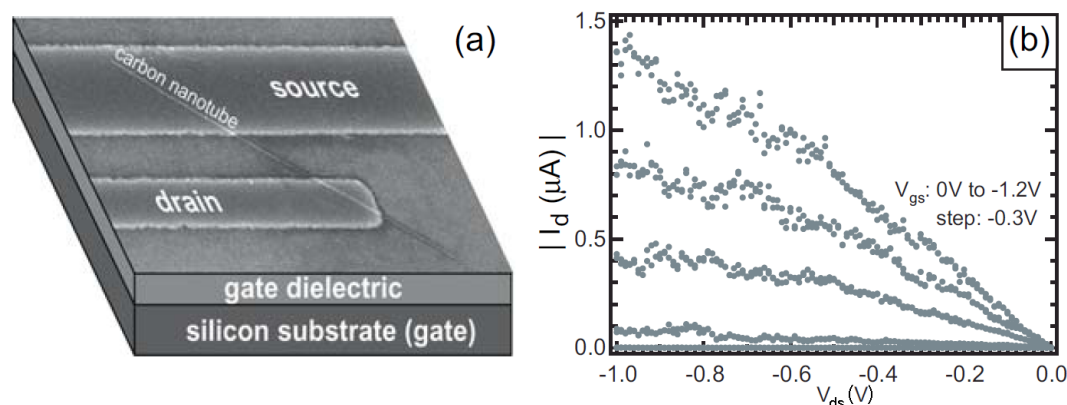


Figure 1.9: (a) SEM micrograph and (b) typical output characteristics of a CNTFET. From [20].

The on-current in a CNTFET is strongly dependent on the specific contact metal. [20] This dependency is plotted in Fig. 1.10, where the current trend follows the work function of the metal: 5.1 eV for Pd, 4.3 eV for Ti and 4.1 eV for Al. [17] For a CNT, the work function is approximately 4.8 eV, close to that of graphite. [21] A higher work function forms a lower Schottky barrier height to the valence band of the CNT, providing a higher on-current. The work functions of the contact metals also govern the gate voltage response of the CNTFET. High work function metals like Pd make good p-type (semiconducting channel opens with negative gate voltage) contacts, while low work function metals like Al yield better n-type (positive gate voltage opens channel) contacts. [3]

The gate voltage can be applied by an universal backgate, usually the silicon substrate, or a local gate, a nearby electrode insulated from the CNT by a thin dielectric layer. In addition to regular FET operation, it is possible to construct CNTFETs modulated with an optical signal by coating the CNT with an optically responsive agent. [22] Chemical gating is also a possibility with the possible application of using exposed

tubes as chemical sensors. Concerning particular gases, NO_2 has been found to shift the threshold voltage positively and NH_3 negatively. [23] Using different contact metals, it is possible to realize both n-type and p-type regions, even on a single CNT. This approach has been used to produce a CMOS-type oscillator with five n-type and five p-type FETs on a single SWCNT. [24]

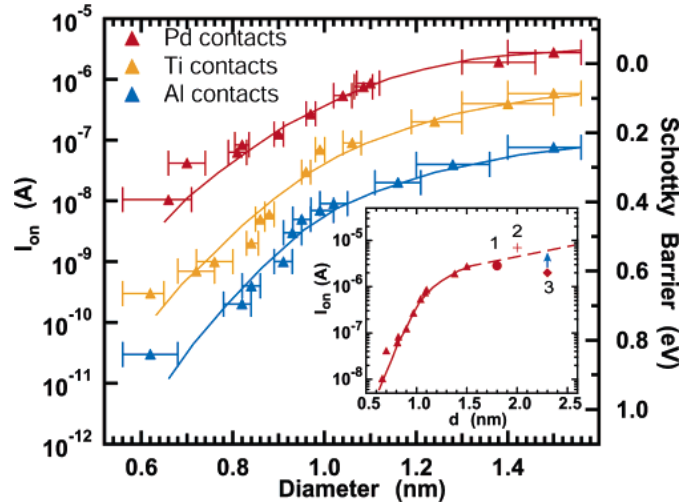


Figure 1.10: The current in the ON-state of CNTFETs as a function of nanotube diameter for contacts made of different metals with the corresponding Schottky barrier. The gate dielectric layer is 10 nm SiO_2 , the channel length is 300 nm and a bias voltage $V_{ds} = -0.5$ V is applied. The inset shows additional data for Pd contacted CNTFETs from other sources. From [17].

1.3.2 CNTFET memory elements

Carbon nanotube FETs often display some degree of hysteresis in their transfer characteristics. Examples of this are in Fig. 1.11, where the CNTFET can be set to different states of conductivity depending on the previous modulation with gate voltage. For normal transistor operation this is an unwanted feature, causing unpredictability in its output. However, the hysteresis effect can be applied in using a CNTFET as a memory device. [25]

The devices produced in this thesis work were used in a study [1] about environmental influences on the operation of CNTFETs as memory elements. The dielectric layers were selected to produce a relatively constant hysteresis effect in the devices. [26]

Several different models have been suggested to explain the origin of hysteresis in CNTFETs. Surface chemistry, for instance water molecules, on the dielectric has been shown to give a large contribution to hysteresis in some CNTFETs. Mobile ions and charges within the dielectric layer (especially in SiO_2) can relocate in response to the

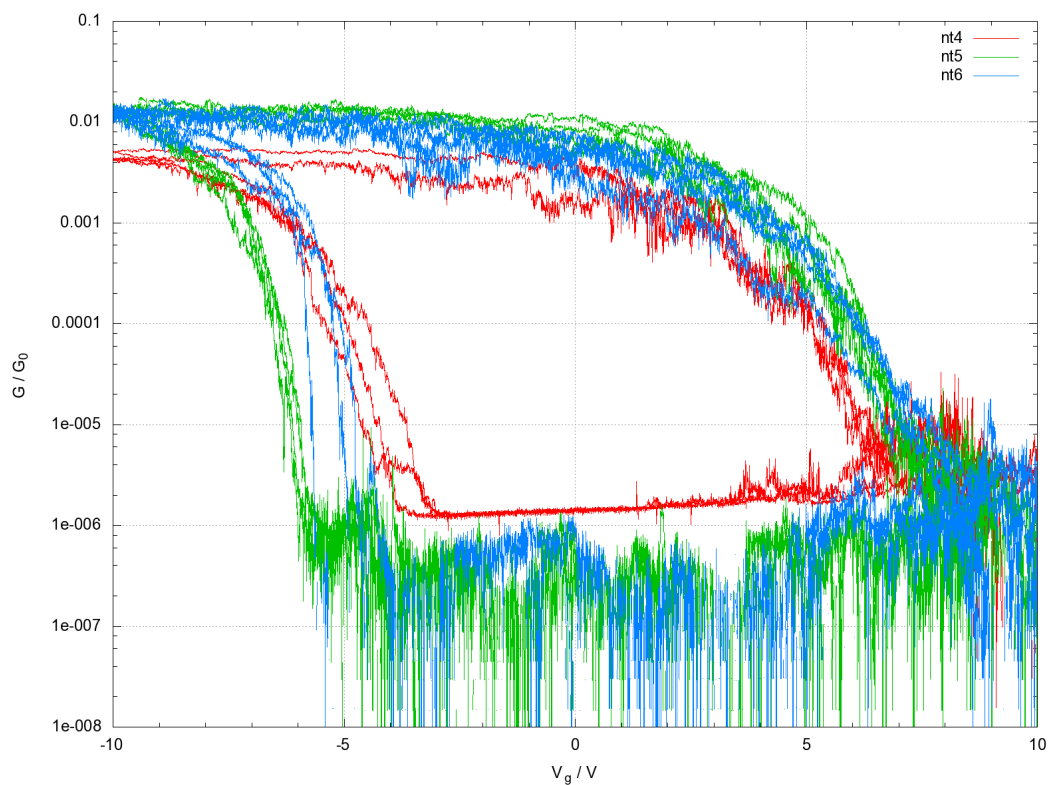


Figure 1.11: Gate sweep curves of adjacent CNTFETs on a Si substrate with a 300 nm SiO₂ gate dielectric layer ($V_{ds} = 10$ mV). The devices have Pd electrodes, producing p-type behaviour. The gate voltage is swept back and forth and the curve is drawn counterclockwise, i.e. changing the gate voltage to a positive value and back sets the device to the on-state with high conductivity. Devices produced (not via DEP) and measured by the author.

gate voltage, which is the reason hysteresis is sometimes visible in conventional Si-MOSFETs. Additionally, charging centers such as defects in the nanotube might cause hysteresis when charged or discharged due to gate modulation. Stationary charge traps within the dielectric could also affect the charge transfer of the CNT in response to the gate modulation, screening the electric field and causing apparent hysteresis in the gate voltage response. [10] With a certain structure of oxide layers a predictable hysteresis effect with CNTFETs can be achieved. This finding points to stationary charge traps in the layered dielectric dominating the electrostatic charging, but surface chemistry also has a significant effect. [26]

Chapter 2

Dielectrophoresis

Charged particles can be moved simply by using an electric field, in which the particles experience the Coulomb force in the direction of opposite charges. This process is referred to as electrophoresis. [27] Neutral particles do not experience a force in a uniform electric field, but nonuniform electric fields can be used to exert forces on polarizable particles. [28]

In an electric field surface charges are induced on a polarizable particle with opposing polarities on opposing sides. The Coulomb force on each of the sides depends on the magnitude of the charge and the electric field. If the field is homogeneous and the overall charge of the particle is zero, the forces on different sides are equal in strength but opposite in direction, so there is no resulting net force. If the field is not uniform, there will be a net force, illustrated in Fig. 2.1. A high nonuniformity in the electric field is desirable for moving particles, a method known as dielectrophoresis (DEP). [28]

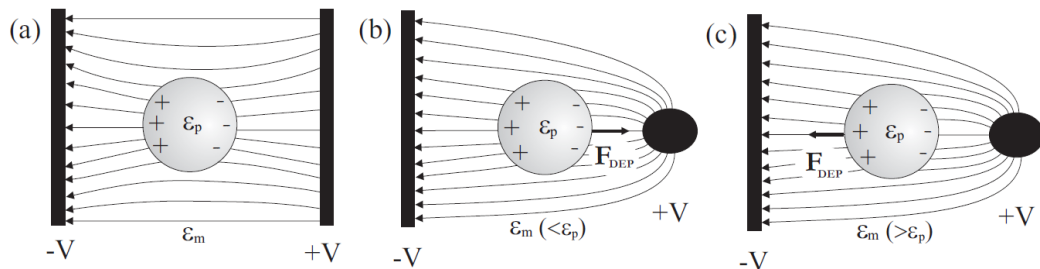


Figure 2.1: A schematic of a neutral particle in a uniform electrical field (a) and in a non-uniform field with the permittivity of the particle ϵ_p larger (b) and smaller (c) than the permittivity of the medium ϵ_m . In positive DEP (b) the particle is moving towards the electric field maximum and in negative DEP (c) the minimum. From [29].

This process does not require any time dependence in the electric field, but even a small charge in the particles can mean that the electrophoretic force dominates in the experiment. Therefore a high frequency alternative current is usually used in DEP, which eliminates the electrophoretic force due to time-averaging. [30]

2.1 Dielectrophoretic force

A particle in an electric field \vec{E} and the surrounding medium can be considered as a dipole with an induced dipole moment [31]

$$\vec{p} = \alpha \vec{E} \quad (2.1)$$

where α is the effective polarizability of the particle, which depends on the frequency of the electric field, the particle radius and the electrical properties of the particle and the medium. In this derivation also the polarization of the medium is taken into account. The polarizability is

$$\alpha = 3V\epsilon_m \text{Re}[K], \quad (2.2)$$

where V is the volume of the particle and ϵ_m is the permittivity of the suspending medium [32]. $\text{Re}[K]$ is the real part of the Clausius-Mossotti factor

$$K(\omega) = \frac{1}{3} \frac{\epsilon_p^* - \epsilon_m^*}{\epsilon_m^* + A(\epsilon_p^* - \epsilon_m^*)}. \quad (2.3)$$

Here A is a geometrical factor ($A = \frac{1}{3}$ for a sphere, $A \approx 0$ for a straight rod with a negligible thickness) and ϵ_p^* and ϵ_m^* the complex permittivities of the particle and the medium. The complex permittivity is defined as

$$\epsilon^* = \epsilon - i \frac{\sigma}{\omega} \quad (2.4)$$

where ϵ is the permittivity and σ the conductivity for the entity in question. ω is the angular frequency of the applied electric field. [32]

The dielectrophoretic force applied to the particle by the nonuniform electric field is [31]

$$\vec{F}_{DEP} = (\vec{p} \cdot \vec{\nabla}) \vec{E} = \frac{\alpha}{2} \vec{\nabla} (|\vec{E}|^2) \quad (2.5)$$

The last expression of the previous equation can be justified with Eq. 2.1 and because the curl of the electric field is zero. [33] The time-averaged dielectrophoretic force for a homogenous sphere in an electric field with a sinusoidal time dependence is therefore

$$\vec{F}_{DEP-tav}^{sph} = 2\pi\epsilon_m r_p^3 \text{Re} \left\{ \frac{\epsilon_p^* - \epsilon_m^*}{\epsilon_p^* + 2\epsilon_m^*} \right\} \vec{\nabla} \left(|\vec{E}_{RMS}|^2 \right) \quad (2.6)$$

where \vec{E}_{RMS} is the root-mean-square value of the electric field. This equation is also valid with a field without a time dependence.

Equation 2.5 shows that the DEP force is parallel to the gradient of the square of the electric field. The direction of the force depends on the relative polarizabilities of the particle and the medium, but not on the direction of the electric field.

Fig. 2.2 shows an example of the frequency dependence of the Clausius-Mossotti factor. The imaginary part of the factor is only relevant for torque in electrorotation, while the sign and magnitude of the real part determine the direction and the magnitude of the DEP force.

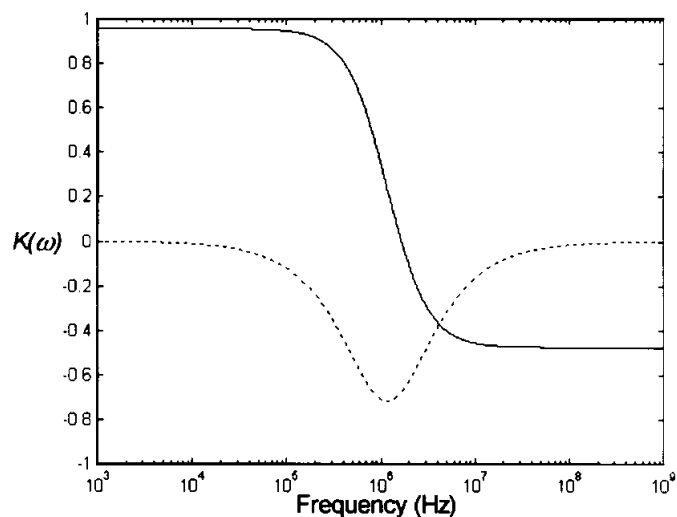


Figure 2.2: The real (solid curve) and imaginary (dotted curve) parts of the Clausius-Mossotti factor. The magnitude and signs of the real and imaginary parts govern the magnitude and direction of the dielectrophoretic force and electrorotational torque, respectively. The frequency-dependence of a solid particle exhibiting a single dielectric dispersion is shown, an example from [32].

For a straight carbon nanotube with a volume V an approximate time-averaged DEP force can be calculated by assuming $A \approx 0$ as

$$\vec{F}_{DEP-tav}^{rod} \approx \frac{3}{2} V \epsilon_m \text{Re} \left\{ \frac{\epsilon_p^* - \epsilon_m^*}{3\epsilon_m^*} \right\} \vec{\nabla} \left(|\vec{E}_{RMS}|^2 \right). \quad (2.7)$$

2.2 Dielectrophoretic potential

Dielectrophoretic trapping can also be described by defining a DEP potential. A force is equal to the negative gradient of potential energy, so DEP potential can be calculated from Eq. 2.5 as [33]

$$U_{DEP} = -\frac{\alpha |\vec{E}|^2}{2}. \quad (2.8)$$

If Brownian motion is also considered, the total potential energy for objects in DEP can be expressed as a sum of thermal and DEP potentials as

$$U_{\Sigma} = U_T + U_{DEP} = \frac{3k_B T}{2} - \frac{\alpha |\vec{E}|^2}{2}. \quad (2.9)$$

The DEP force pushes the polarizable particles to wells in this potential, and trapping happens when $U_{\Sigma} \leq 0$ i.e. the DEP force overcomes the random thermal motion. [29]

2.3 Electric fields in DEP

An electric field through a dielectric material that contains no free charge has zero curl (the direction of the field acts outward from a point). Additionally, if the electric field is applied externally to the dielectric, the field is not divergent. [34] Mathematically

$$\nabla \times \vec{E} = 0 = \nabla \cdot \vec{E}. \quad (2.10)$$

With these conditions the electric field in free space can't contain isolated maxima, which means in practice that the field is always greatest on the surface of electrodes. There can, however, be any number of isolated field minima in free space. As positive dielectrophoresis moves particles toward a greater field strength, the particles will gather at the electrodes. With negative dielectrophoresis the electrodes can be designed to produce a field minimum where the particles will be trapped. [34]

Simulations for a typical DEP setup are shown in Fig. 2.3. The gradient of the electric field is greatest at the sharpest tips of the electrode structure.

2.4 Brownian motion

In addition to the DEP force Brownian motion is a relevant factor in the movement of nanoscale particles. This can be treated as a random force approximated by

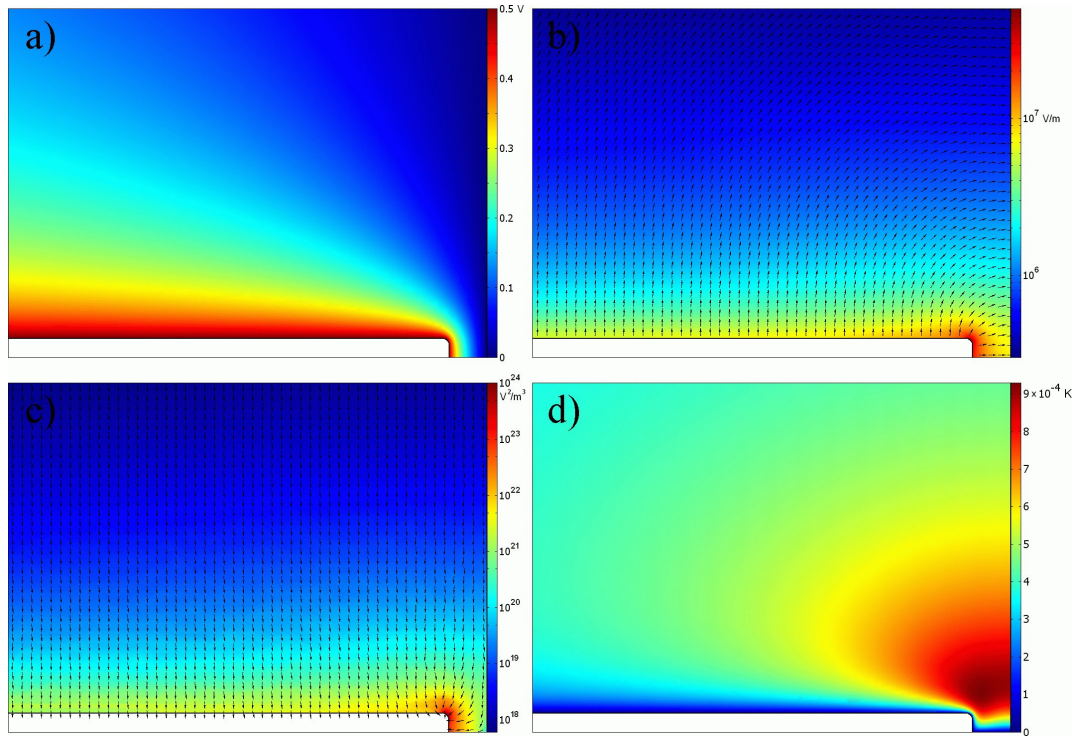


Figure 2.3: Calculated plots for a DEP experiment showing a) electric potential, b) electric field, c) gradient of the electric field square and d) temperature rise. The plane is perpendicular to the substrate, going through the center axis of a straight electrode. The setup has two symmetric electrodes, and the amplitude of the voltage across the gap (80 nm width) is 1 V, AC frequency 12.5 MHz and the conductivity of the liquid surrounding the electrodes $300 \mu\text{S}/\text{cm}$. The width of the displayed area is 500 nm and the height is 360 nm. Electrode thickness is 20 nm and width 25 nm. The directions of vector quantities are displayed with arrows. From [27].

$$F_{thermal} = \frac{k_B T}{2r_p}, \quad (2.11)$$

where k_B is the Boltzmann constant, T temperature and r_p the radius of a spherical particle. Since smaller particles experience a higher thermal drag force, they need steeper electrical field gradients in DEP experiments. [28]

Considering thermal effects, the critical particle radius for a DEP trapping experiment can be represented as

$$r > \sqrt[3]{\frac{10k_B T}{\pi\epsilon_m \Delta d \operatorname{Re}[K(\omega)] \nabla E^2}}, \quad (2.12)$$

where Δd is the trap width. [34] This sets a minimum scale for particles where DEP overpowers thermal effects. Generally DEP is most useful for particles with length scales between 1 μm and 1 mm, the upper limit determined by gravity. An example of the critical radius dependence on the trap width and electric field gradient is in Fig. 2.4.

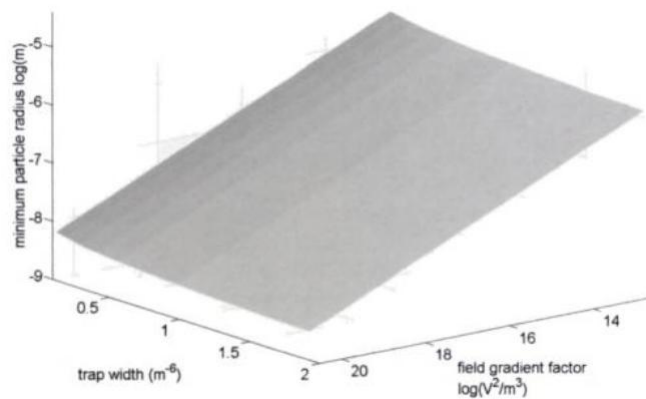


Figure 2.4: The minimum radius of particles that can be trapped using DEP using Eq. 2.12. The parameters used are $T = 300$ K, $\epsilon_m = 78\epsilon_0$ and $\operatorname{Re}[K(\omega)] = 1$. Plot from [34].

2.5 Fluid dynamics

The fluid flow in a system with electrodes providing nonuniform AC electric fields in a fluid medium is caused principally by three effects. Electrothermal fluid flow is caused by the thermal gradient produced by the electric fields in the system. The second component, AC electro-osmotic (ACEO) fluid flow, stems from the interaction of ions in an electrical double layer on the electrode surfaces with the tangential component

of the electric field. Natural convection can also exist in the fluid, driven by density differences in the fluid caused by thermal expansion. [27]

The electrothermal flow is by itself in a DEP experiment much slower than the ACEO flow. Typically the electrothermal flow has maximum speeds in the range of 10 nm/s to 1 $\mu\text{m/s}$ while ACEO flow speed can reach 10 cm/s. [27] [35]

The direction of the ACEO flow is always perpendicular to the electrode edge with an AC voltage, driving fluid on the electrode surface. The direction of the flow is not dependent on the sign of the electric field. [36]

The fluid flow in a DEP setup has been numerically evaluated in Fig. 2.5. The flow goes generally into the gap from the sides and the top, proceeding out along the electrodes.

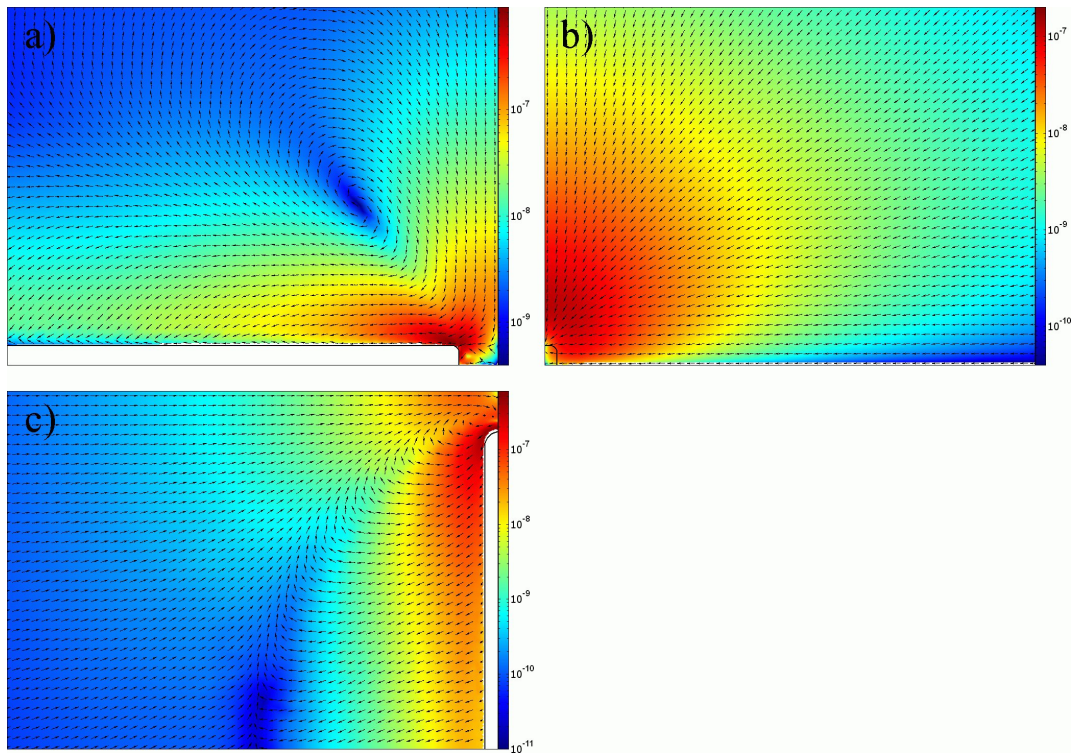


Figure 2.5: Electrothermal fluid flow simulation for a DEP experiment. a) Plane perpendicular to the substrate at the axis of an electrode (as in Fig. 2.3), b) plane perpendicular to both the substrate and the electrode axis, c) plane parallel to the substrate at a height of 10 nm. The unit of velocity is m/s. Electrode dimensions are as in Fig. 2.3. $V = 1 \text{ V}$, $f = 1 \text{ MHz}$ and liquid conductivity $\sigma = 300 \mu\text{S/cm}$. The width of the displayed area is 500 nm and the height is 360 nm. Simulations done in [27].

2.6 Applications

Dielectrophoresis has been used in separating and trapping micron-sized objects such as cells. Separation of particles by structure and composition can be done by spatially confining them by negative DEP into a static reservoir or focusing them in a fluid flow. [37] Trapping the suspended objects with positive DEP to electrode surfaces in stagnant or flowing liquid is another method for this, but for larger quantities a different setup with moving liquid can be used.

Field-flow fractionation (FFF) using DEP is based on the DEP force as a function of the dielectric properties of a particle as well as the particle sedimentation force and the hydrodynamic lift force. In a laminar flow chamber the flow velocity parallel to the chamber walls is dependent on height relative to the electrodes producing the electric field. This difference in velocities can be used to separate different particles. [38]

There are three primary modes of velocity differentiation in FFF, where different force fields can be used for positioning particles in the stream. Normal FFF is based on thermal diffusion profiles of particles with sizes below $1\ \mu\text{m}$. For larger particles Brownian motion and thermal diffusion are roughly negligible. In steric FFF the applied force causes particles to hit one side of the separation chamber with steric hindrances slowing the particles down. Hyperlayer FFF is based on keeping particles on an equilibrium height away from the chamber walls in the flow stream. [37]

As a nanoscale method, dielectrophoresis can be scaled to be used for manipulation and trapping of different particles such as DNA assemblies [39] and it is also possible to use it as a lithography tool with electrode arrays. [40]

In a configuration commonly used in DEP the circuit consists of a large resistance and an AC voltage source in series with the trapping electrodes. If the particle to be trapped is conductive enough, most of the voltage drop will be in the resistor after the circuit has been closed by the particle. Therefore the electric field at the electrodes will drop and the DEP effect will be diminished for any additional particles. [34] This approach is problematic with the unsorted CNTs used for the experiments presented in this thesis, because one third of the tubes are metallic with significantly lower resistances than those of the desired semiconducting tubes. The trapping would terminate much more effectively with a metallic tube using a resistor in series, so the described approach was not used in the experiments.

The resistance of the trapped particle can also be detected during trapping by using a lock-in amplifier (Fig. 2.6). This involves measuring both I_{AC} and I_{DC} components during trapping to determine the actual resistance between the electrodes. Applying this to single SWCNTs has the advantages of having a verified electrical connection and controlling the amount of resistance during trapping. [41]

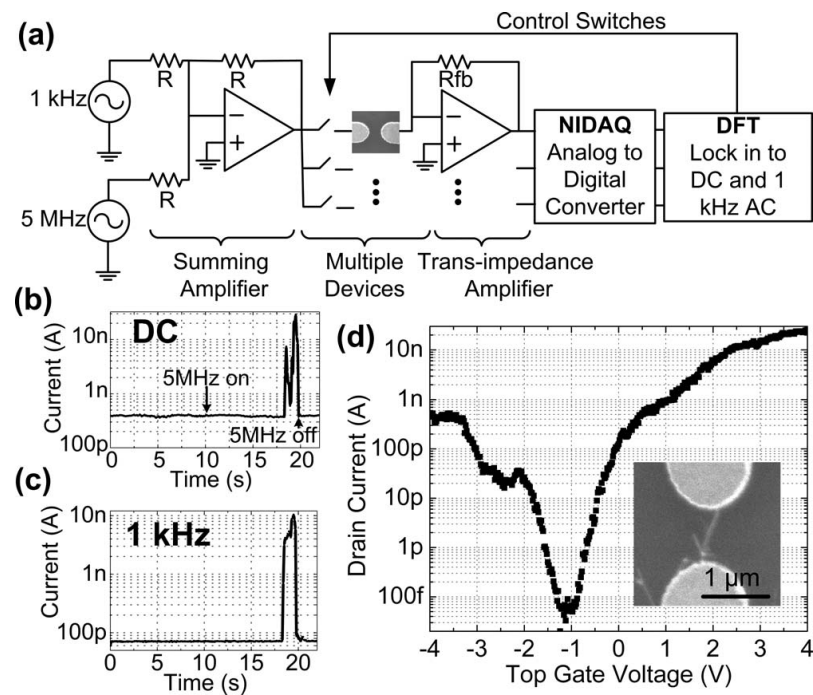


Figure 2.6: a) Lock-in detection setup for DEP. b), c) Real-time current measurements during DEP trapping, showing the effect of deposited particles. d) A gate voltage sweep from a fabricated CNTFET with $V_{ds} = 100$ mV and Au electrodes. Inset shows SEM of the CNT. From [41].

2.7 DEP on CNTs

Both AC and DC DEP have been previously demonstrated to be an efficient method to place CNTs, CNT matted sheets and CNT bundles across prepatterned electrodes. Previous experiments done with two electrodes have often involved producing a film of aligned CNTs, usually on silicon but also on flexible substrates [42].

CNTFETs have been produced with DEP before, but usually with surfactants coating the tubes. Typical surfactants such as SDBS can be removed afterwards by rinsing the sample with methanol. [43] Often the FET is produced with a sheet of CNTs as the semiconducting channel. [44] If a film is used, the device typically does not have a good off-state due to the practically inevitable inclusion of metallic tubes. One method of getting rid of unwanted metallic tubes in bundles or sheets is electrical breakdown. [45]

Dielectrophoresis has also been used to produce CNTFETs with a prefabricated local gate. A local gate offers faster switching behaviour than a global back gate. [46] More complex electrode arrangements can be used to have four point electrical contacts on single nanotubes. These can be used for more exact measurements of CNT properties than two point contacts. A four point deposition yield of 16 % has been achieved for this configuration. [47]

The experiments presented in this thesis use 1,2-dichloroethane (DCE) as the suspension for SWCNTs. The real part of the permittivity of DCE is between different types of CNTs, but with the frequency dependence and conductivity taken into account, the positive DEP case in Fig. 2.1 b) is achieved for $f = 300$ kHz. For semiconducting SWCNTs $\epsilon_{s-SWCNT} = (2-5)\epsilon_0$ [42] and for DCE $\epsilon_{DCE} = 9.8\epsilon_0$ at 31.5 °C. [48] Metallic SWCNTs have high conductivity and have permittivities many orders of magnitude larger than these values.

With relatively low frequencies (< 1 MHz) both metallic and semiconducting CNTs will move towards a direction of higher electric gradient (positive DEP, Fig. 2.7) and so sharp edges in electrodes are expected to gather more particles. The time taken to rotate a SWCNT bundle parallel to the electric field is simulated to be as short as a few milliseconds, but the translation movement time in a typical structure (a distance of a few millimeters) can be tens of seconds. [42]

Different AC frequencies can be used to attract only metallic tubes (> 10 MHz) or both metallic and semiconducting ones. With this effect metallic SWCNTs can be extracted from a suspension by AC dielectrophoresis, [51] also using a fluid flow across an electrode array [52]. In this method the tubes are kept separate with surfactants, which induce a surface conductance. This property gives rise to a frequency dependence of the nanotube dielectrophoresis. [53]

Crossed nanotube junctions have been produced using DEP, but with tubes coated with the surfactant sodium dodecylbenzene sulphonate. The deposition was done sequentially, but with sharper tips than in four-electrode attempts for this thesis. [54]

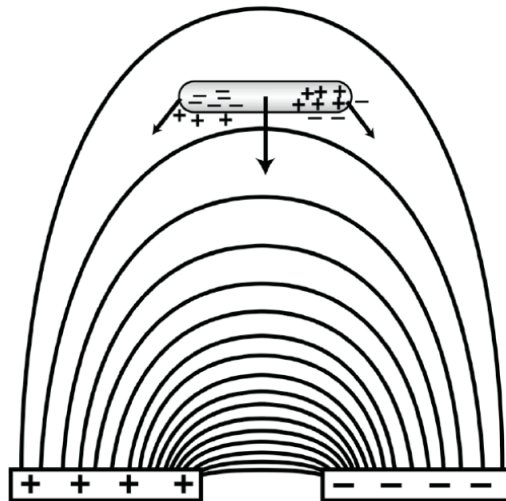


Figure 2.7: A carbon nanotube in a medium subjected to dielectrophoresis. The DEP force direction for positive DEP is shown. From [49] via [50].

Resistive sensing elements have also been fabricated using DEP with CNTs. The I - V curves of the tubes are sensitive to temperature and humidity, which is useful for nanoscale measurements with a very small power dissipation. [55]

Chapter 3

Sample fabrication

3.1 Substrate

The sample base used in the experiments was monocrystalline silicon. The size of the silicon chip containing one sample was 4 mm by 4 mm and the substrate thickness was 300 μm . The edges of these squares were shallowly cut in the substrate with a dicing saw (LoadPoint MicroAce 3) before sample fabrication to ease sample separation in the wafer. Usually 20–30 samples were made in one batch, an amount limited by the size of the electron microscope sample holder (28 mm by 28 mm). The tilt of the sample also limits the area of accurate electron beam exposure, as the focus height of the beam cannot practically be changed without stopping the batch exposure manually.

Different ALD layers were grown on the samples at Planar Systems Inc. (currently Beneq) in Espoo using a Planar P400A ALD deposition tool [56]. In sample batch DEP4 the coating was ALD #2107 with the layers from bottom to top HfO_2 40 nm, TiO_2 0.5 nm and HfO_2 1 nm [57]. These oxides were used as a gate dielectric layer.

3.2 Electrode design

The design of the electrode tips was kept constant in all sample batches. The gap between electrodes was 1 μm and the width of the electrodes near the tip was a constant 300 nm. In the design program the tip point had a 90° angle with straight edges extending symmetrically. In practice this design produced a rough half-circle at the tip. The positions of the gaps relative to each other differed between sample batches. In batches DEP3 and DEP4 the gaps were placed symmetrically in a circle to eliminate any effect relating to different electrode positions between gaps (Fig. 3.1).

3.3 Electron beam lithography

The first step in fabricating the DEP electrodes was spinning the resist layers on the substrate. In electron beam lithography PMMA (polymethylmethacrylate) is the most

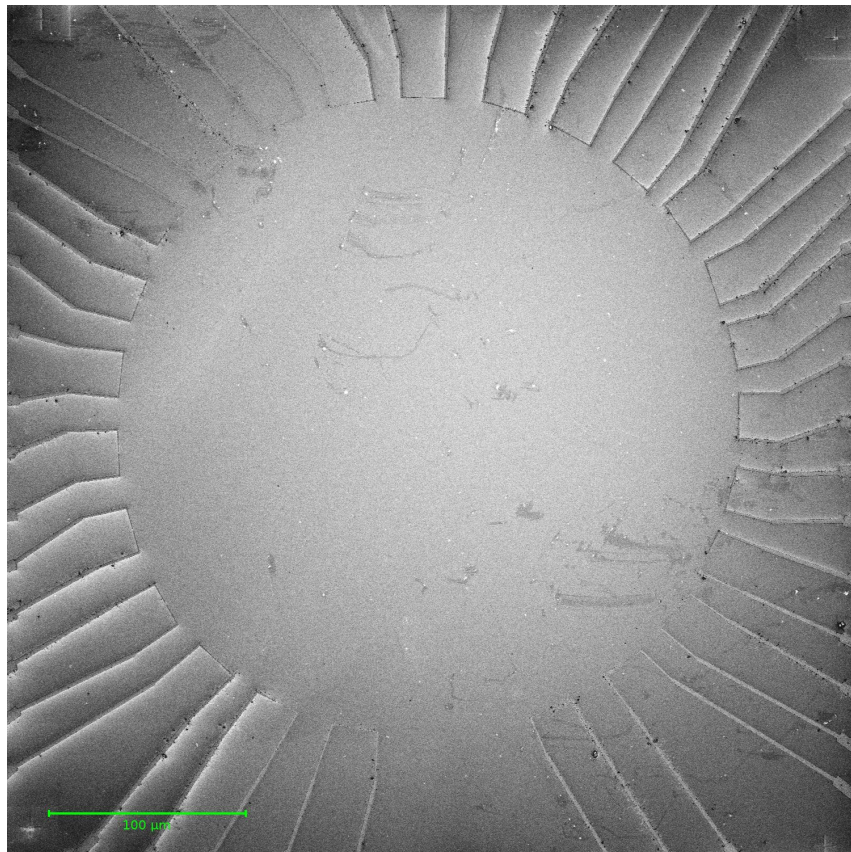


Figure 3.1: The configuration of the trapping electrodes used in sample batch DEP4 (DEP4_18). The diameter of the circle is $320 \mu\text{m}$.

common resist, and two layers of it were used in this project. The spinner used was Bidtec SP100. The first layer was PMMA with a molecular mass 495 u , concentration 3% in anisole. The spin speed was 3000 rpm, which produces a layer with a thickness of 100 nm. After spinning the sample was baked on a hot plate at 170 °C for 5 minutes. The second layer was 950 u PMMA, 2% in anisole. The spin speed 6000 rpm results in a 80 nm layer and the sample was baked again with an identical procedure.

The electrical circuit was drawn with a Raith e_Line 50 electron beam lithography system. The electron beam acceleration voltage used in drawing the patterns was 20 kV and the typical current dose was 200 $\mu\text{As}/\text{cm}^2$. The fine pattern in the center was drawn with a 30 μm aperture and the outer electrodes and bonding pads with a 120 μm aperture. The larger aperture allows for a higher current and therefore a shorter exposure time, but can't be used for small structures due to a larger beam spot size.

Exposed parts of the resist were removed in a developer solution of 1 part of MIBK and 3 parts of IPA. After development the PMMA layers were cleaned with oxygen plasma in a Oxford Plasmalab 80 Plus reactive ion etching (RIE) system. The recipe used in this specified a time of 10 s, a power of 15 W and a magnetic flux density of 30 mT. The O_2 flow was 50 cm^3/min .

Two different metal layers were evaporated on the sample with a BAL-TEC BAE 50 electron beam vacuum evaporator. A 5 nm titanium layer was used to bond the 25 nm palladium layer to the surface. The layer thicknesses were measured during evaporation using an Inficon deposition controller XTC/2.

After metal evaporation the PMMA layers were removed with excess metal in acetone. The lift-off was aided usually by heating the solvent and using ultrasonication.

After checking the electrode structure under an optical microscope, the samples were cracked apart along the grooves cut in the substrate. These separated samples fit in a chip carrier, which provides electrical connectors for the measurement box. The bottom of the sample was glued to the carrier with varnish and an ultrasonic bonder was used to connect the bonding pads of the electrode structure to corresponding chip carrier connectors (Fig. 3.2). The wire used in bonding was a 20 μm gold wire.

In sample batches DEP1 and DEP2 the general concept of DEP was tested with a large array of DEP electrodes but only two bonded electrical contacts. Batches DEP3 and DEP4 used a two-electrode configuration and batches DEP5-10 a four-electrode one. The electrode placement in batch DEP4 is shown in Fig. 3.1.

In batches DEP5-DEP10 the electrodes were facing the gap in four directions (Fig. 3.3). In batches DEP6-DEP10 an additional 60-65 nm Al_2O_3 layer was used to prevent direct electrical connections between the electrode structures and the back gate. These samples also had a 7 nm chromium layer instead of titanium for bonding the layers to each other.

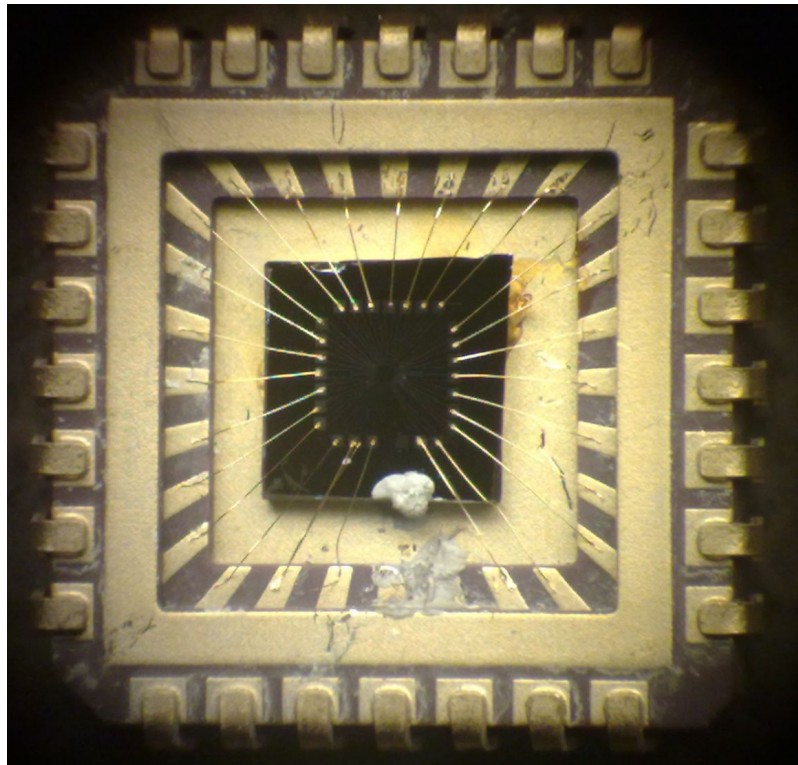


Figure 3.2: A DEP sample (DEP4.22) attached and bonded to the chip carrier. The sample dimensions are $4\text{ mm} \times 4\text{ mm}$ and the silicon base is electrically connected to the bottom of the carrier and two connectors with silver paint.

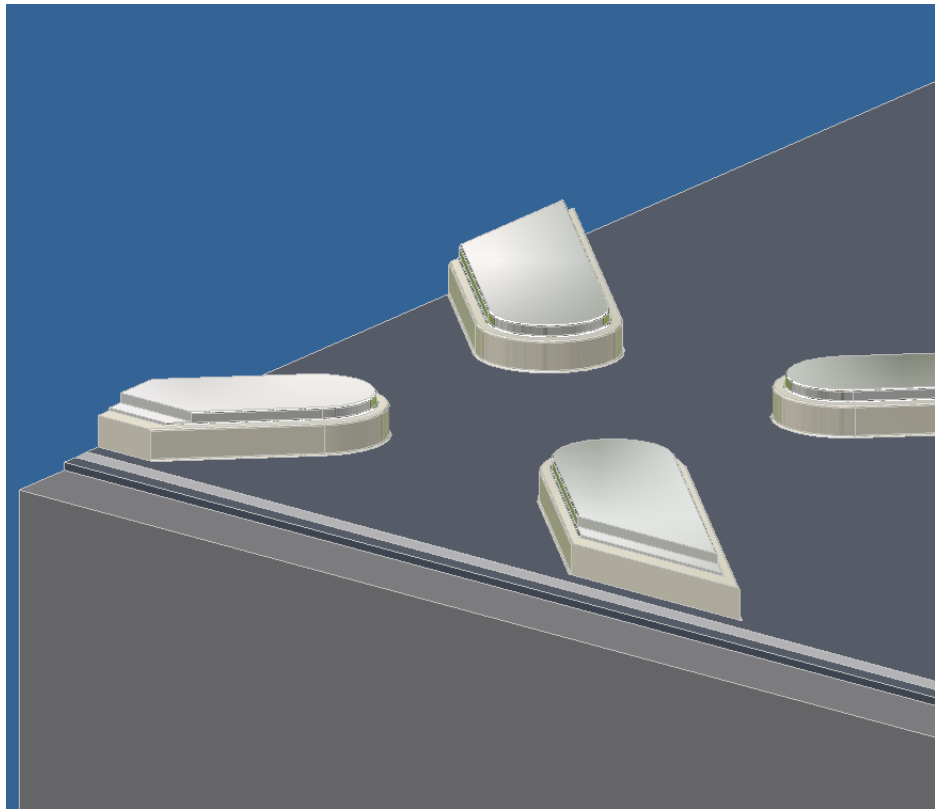


Figure 3.3: The structure of batch DEP8 without CNTs. Layers from the bottom to the top: Base Si, ALD-layers 20 nm HfO₂, 0.5 nm TiO₂, 0.5 nm HfO₂. Below the electrodes 80 nm Al₂O₃, electrodes 7 nm Cr, 25 nm Pd. Gap between electrodes 1 μm, electrode width 300 nm. The layer thicknesses and electrode sizes are to scale.

Chapter 4

CNT trapping

4.1 CNT preparation

The CNTs used in the trapping experiments were single-walled and manufactured by NanoCyl S.A. (Sambreville, Belgium) using catalytic CVD. [56] A small amount of the CNT material, sold as a black powder, was suspended in 1,2-dichloroethane (DCE). The root suspension included 1.5 mg of the powder and 19.15 g of 1,2-dichloroethane. This was diluted with DCE so that the mass concentration of the CNT material was between 1:98000 and 1:270000 when used for DEP in sample batch DEP4.

Because no surfactants were used, the CNTs in the suspension had a high propensity to bundle to each other. A finger sonicator was used to separate the bundles (Hielscher UP400S Ultrasonic Processor). The sonication time used was between 30 minutes and 3 hours depending on the sample batch, and the sonicator was used at full power with about 1 second cycles (half a second on, half a second off).

4.2 Experiment setup

The chip carrier with the sample was placed in a slot inside a measurement box with appropriate electrical contacts and shielding. The electrodes on the sample were connected through the chip carrier and measurement box to BNC connectors, where cables from AC signal sources were inserted.

Three different signal generators were used: Agilent models 33220A and 33250A as well as Tektronix AFG3102 with two generators used at the same time. An oscilloscope (Tektronix TDS3012) was used to check the phases of the alternating current. The whole experiment setup was inside a fume hood to limit exposure to dichloroethane fumes.

In sample batch DEP4 a sine curve signal with a peak-to-peak voltage $V_{PP} = 5$ V was used. The frequency was 300 kHz and trapping time 2 min. Similar parameters have been used elsewhere with an aqueous CNT solution with surfactants, [43] and the frequency is much lower than the one reported for trapping only metallic SWCNTs (10

MHz). [51] The connectors in the box were set up so that every other electrode got a signal from one signal generator and the other half used the second generator as in Fig. 4.1 a). Using the oscilloscope the signals were first adjusted to be in opposite phases (Fig. 4.1 b)).

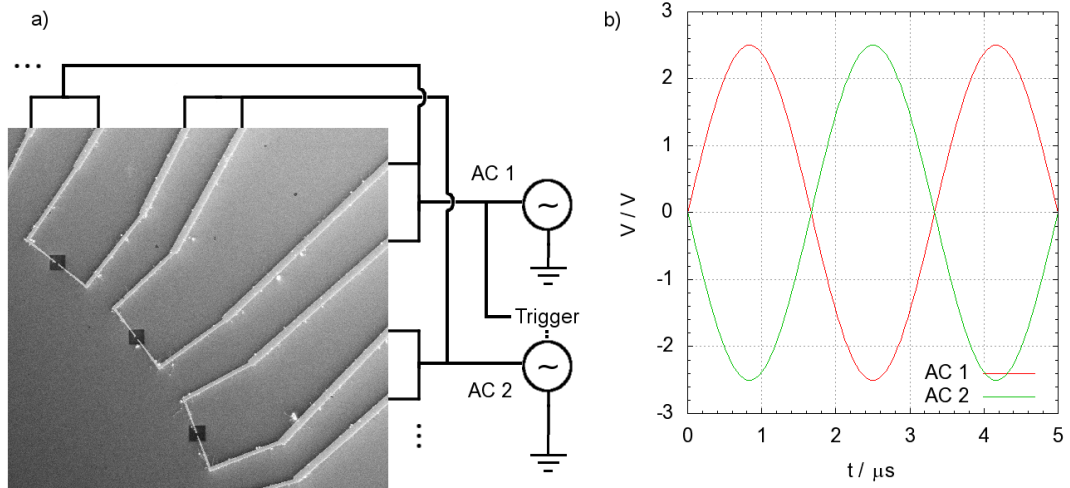


Figure 4.1: a) DEP trapping circuit. The signal generator AC 2 is triggered from the first signal generator (AC 1) output at a rate of 3 kHz to keep the AC voltages synchronized. b) Plot of AC outputs at $f = 300$ kHz and $V_{PP} = 5$ V.

The connectors were disconnected when the sonicated CNT suspension was applied on the sample using a pipette. When the sample surface was completely immersed in the suspension, the signal generators were connected to the measurement box. The signal was applied for 2 minutes and the signal generators were again disconnected.

As the DCE evaporated during the experiment, new drops of the CNT suspension were applied to prevent drying. The number of drops was between 5 and 8 depending on the evaporation rate. After disconnection, the remaining suspension was blown to the side with a helium stream. The suspension pooled around the sample in the chip carrier, and the helium stream was continued until the whole carrier appeared dry.

Chapter 5

Results

5.1 CNT placement

The location of individual nanotubes on the samples was checked using SEM micrographs. In figure 5.1 the top electrode had an AC signal during DEP while the bottom one was disconnected. The HfO₂ surface was generally free of CNTs and debris. It was obvious that the AC signal had an effect on CNT placement. Those electrodes that had the voltage signal applied had CNTs and other material from the suspension attached to them.

A finding common to all sample batches was that the gaps between electrodes did not have a higher density of tubes after trapping than other electrode edges. The cleanliness of the surface in the DEP experiments indicates that most of the suspension material close to the electrodes is deposited to the electrodes themselves.

Different DEP parameters for frequency, voltage amplitude and trapping time were tested in batches DEP1 to DEP3. The resulting parameters were used in batch DEP4.

5.1.1 Two-electrode configuration

In sample batch DEP4 a total of 22 samples were used in DEP experiments. Each sample had 25 gaps which had a different electrical contact on each side. The DEP method on these samples involved applying 5–8 drops of CNT suspension on an individual sample and having the AC voltage on typically for 120 seconds. The concentration of the CNT suspension differed, however, between DEP sessions.

By tuning the trapping parameters a yield of 28 % was achieved in contacting the two electrodes with a single nanotube in the best sample, but the overall success rate with this metric was 12.5 % (Table 5.1), when counting only the first time trapping was attempted on a sample. Some samples were cleaned with RIE and trapping was attempted again (marked with c). If these are included, the total yield was 14.3 %. The contact between electrodes was evaluated with SEM micrographs. Subsequent electrical measurements showed that a sufficient electrical contact was lacking in most

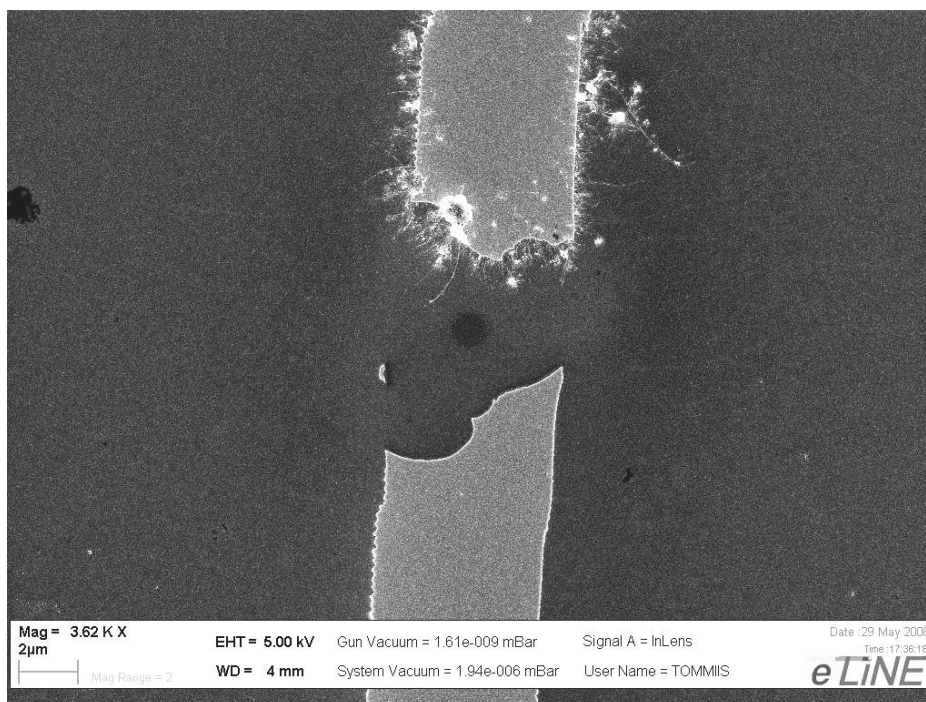


Figure 5.1: A broken electrode with the upper part connected to the signal during DEP, sample DEP4.22.

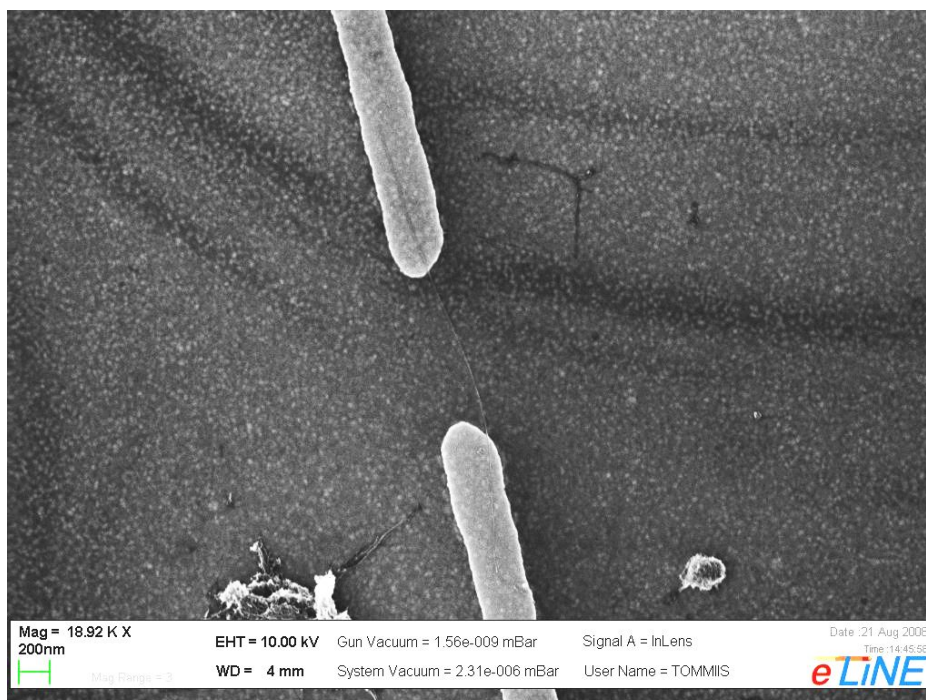


Figure 5.2: A CNT placed between two electrodes with DEP, sample DEP4.17r, gap 21.

cases.

When comparing different concentrations, the lowest one during the last trapping involving cleaned samples was the most successful, having a yield of 22% for single tubes.

As the samples were imaged with SEM before electrical measurements, a 1.5 – 2 nm contamination layer was found via AFM imaging (Fig. 5.3). This carbonaceous material is deposited via electron beam-induced contamination. The carbon originates most likely from both the sample itself and hydrocarbons in the SEM vacuum. [58] The pumping system and other internal SEM components are the most common sources of the hydrocarbons. The thin contamination layer becomes more visible when using low accelerating voltages in SEM as in Fig. 4.1 a) around the electrode gaps. [59]

5.1.2 Four-electrode configuration

The aim of the four-electrode configuration was to have two single SWCNTs crossing each other with electrical connections at all four ends. This would give information about the electrical connection between the tubes on top of each other. The connection between two metallic tubes has been seen to behave as a tunnel junction, whereas junctions between a metallic and a semiconducting tube have shown Schottky diodelike behavior. [54] The batches used for this (DEP5–DEP10) have a common electrode configuration, but differ in processing.

In a four-electrode configuration (Fig. 5.4) the DEP voltage was applied to two opposing electrodes in two sessions so that all four electrodes were used. As the CNTs were usually attached in all edges of the electrodes, a clean cross-like configuration of CNTs was not achieved in any of the samples. The most common result was that the nearest electrodes were connected with CNTs as well as the opposing ones.

5.2 FET measurements

The electrical properties of a specific gap between electrodes were determined with a measurement setup (Fig. 5.5), which included two voltage amplifiers, one current amplifier, a voltage box (source for the DC sweeps) and an analog-digital converter card for the PC. The voltage amplifiers measured gate voltage V_g and drain-source voltage V_{ds} while the current amplifier was used to measure drain-source current I_{ds} .

The measurement of a specific device began typically with a V_{ds} sweep. The voltage was changed from 0 V to +0.1 V with 0.5 mV steps every 0.1 s. Next a sweep was made from +0.1 V to -0.1 V to determine the I - V curve of the device. V_{ds} was then swept to +0.01 V, which was the bias during gate voltage V_g sweeps. At this bias V_g was swept to -3 V and then back and forth between -3 V and 3 V. All voltages were changed gradually and higher gate voltages than ± 3 V were not used to prevent damage to the device.

Table 5.1: The distribution of trapped CNTs in different samples in batch DEP4. Each sample has 25 gaps where trapping was attempted. If the total is less than 25, the amount of material could not be determined in all gaps. The final column shows the relative mass concentration of 1,2-dichloroethane in relation to the CNT material. Samples with "centr." had the suspension centrifuged and the upper part of the product used for trapping, resulting in an unknown concentration.

Sample	No material	Tube(s), no contact over gap	One tube over gap	>1 tube or other material	Parts DCE for 1 part CNT
22	5	7	1	12	98000
23	8	7	4	6	98000
24	0	6	3	16	98000
6	15	5	2	3	180000
12	1	1	3	20	180000
13	1	7	2	15	180000
14	8	5	1	11	180000
8	0	6	2	17	180000
9	0	7	3	15	180000
10	0	1	3	21	180000
11	0	10	7	8	centr.
15	0	15	4	6	centr.
16	4	7	6	8	centr.
17	20	4	1	0	centr.
18	4	11	5	5	180000
21	6	7	4	8	180000
25	23	2	0	0	180000
28	22	3	0	0	180000
19	3	6	5	11	140000
20	0	5	5	15	140000
26	0	3	4	18	140000
27	0	5	4	16	140000
6r	6	13	1	5	180000
15r	0	6	1	17	180000
17r	14	5	0	2	180000
17rc	11	3	8	3	270000
18c	20	2	3	0	270000
25c	2	4	8	11	270000
28c	9	10	3	3	270000
1st time	120	130	69	231	
Total	182	173	93	272	

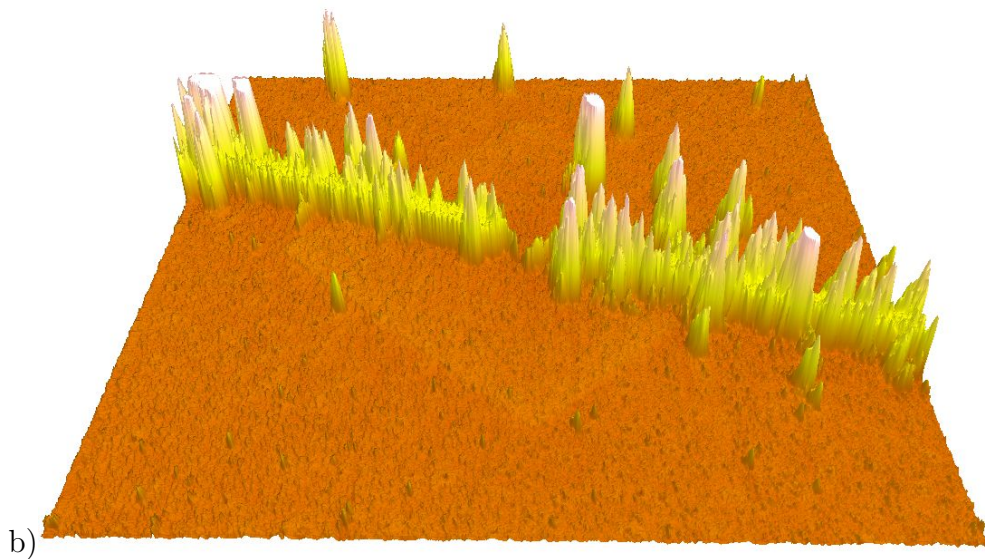
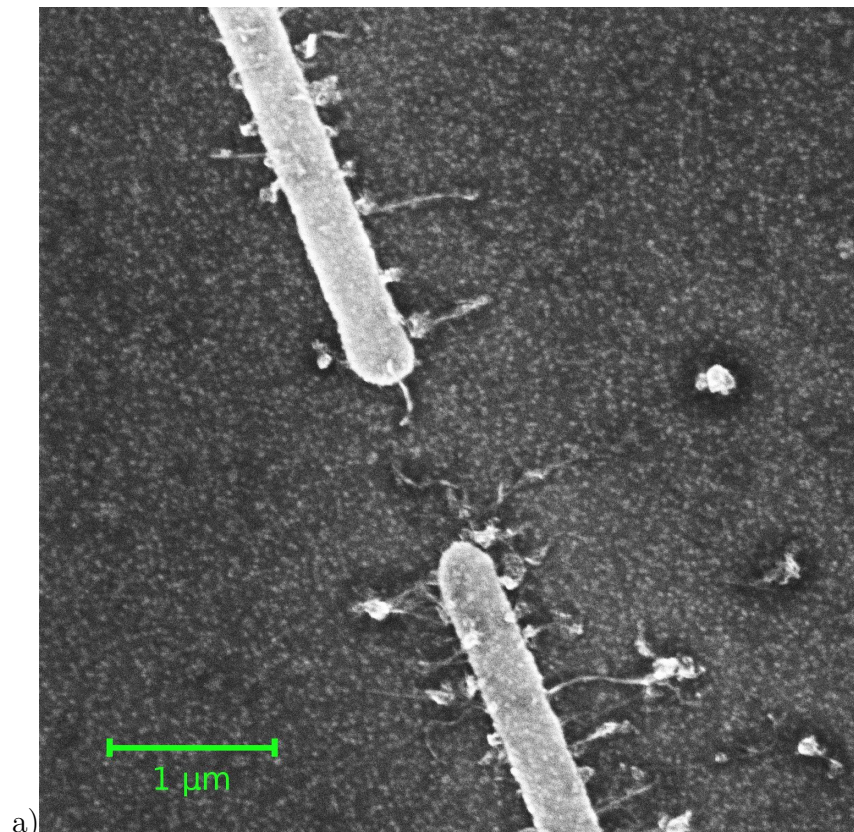


Figure 5.3: a) A SEM image of sample DEP4_16, gap 11. b) The same device imaged with AFM ($10 \times 10 \mu\text{m}$). A 5 by $5 \mu\text{m}$ square is visible in the area imaged previously with SEM. This area rises $1.5 - 2 \text{ nm}$ higher than the rest of the probed area, which is explained by amorphous carbon deposited on the sample in SEM imaging. Because a script was used for SEM imaging, only the square was exposed (acceleration voltage 5 kV , aperture $30 \mu\text{m}$, current 0.33 nA , 1500 lines, total time $\approx 30 \text{ s}$). The electrode height relative to the substrate is 30 nm in smooth areas.

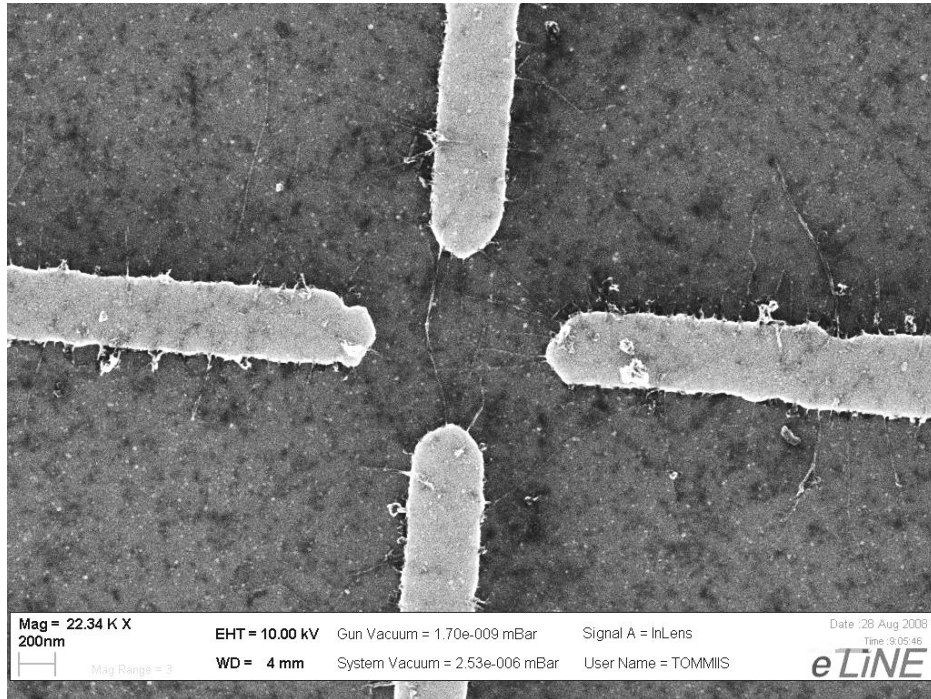


Figure 5.4: A four-electrode configuration with trapped CNTs (sample DEP5_5, device 5).

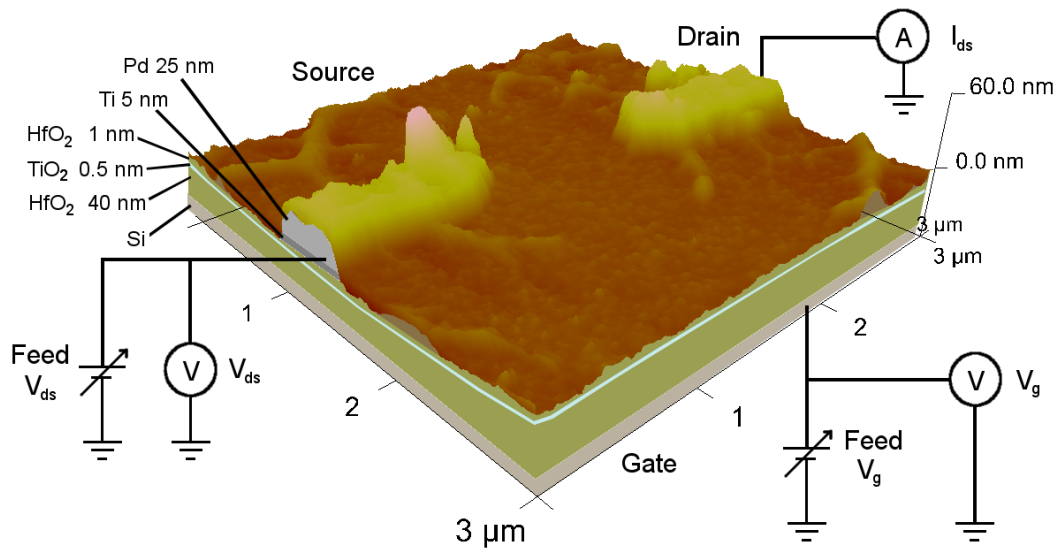


Figure 5.5: Measurement circuit for FET evaluation. AFM micrograph is of sample DEP4_13, gap 1, with layer thicknesses valid for batch DEP4.

Gaps in 15 different samples were measured, usually those that had at least one tube connecting the electrodes in SEM micrographs. Most devices did not show a response typical for a CNTFET, but a significant percentage did (Fig. 5.6).

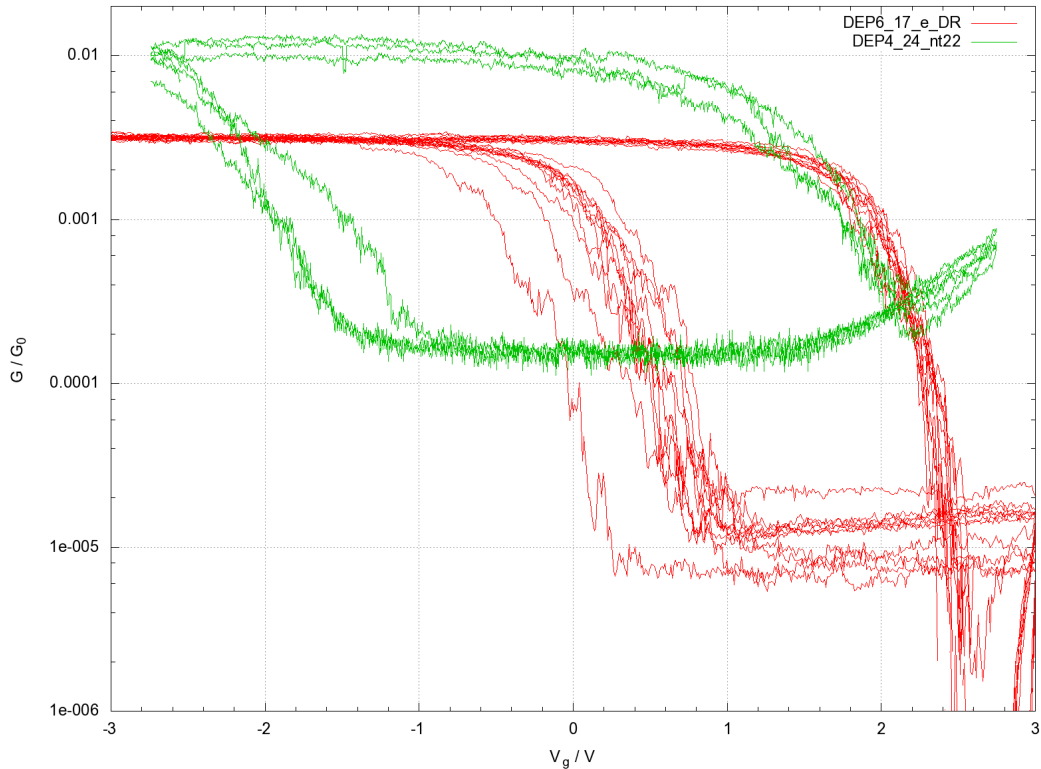


Figure 5.6: The transconductance of two CNTFETs produced via DEP during several gate voltage sweeps ($V_{ds} = 10$ mV). Both devices have a clear hysteresis, which produces a curve in the counterclockwise direction, and the DEP4 device also has a slight n-type behaviour at positive gate voltages in addition to the normal p-type response.

The ratio between on- and off-states for the 48 fabricated devices was 50 at most (Fig. 5.6, DEP4.24), usually between 1.1 and 2. Other CNTFETs fabricated without DEP have yielded ratios up to 10000. The semiconducting channel in DEP fabricated devices does not seem to close correctly, which is possibly explained by the carbon contamination layer on the samples produced by SEM imaging. The samples were not generally cleaned after SEM imaging, and RIE processing necessary to remove the amorphous carbon would have also damaged the CNTs at a similar rate.

Using a resistivity value of $\rho_C = 1.35 \times 10^{-5}$ Ωm for carbon [60], a classical calculation [61]

$$R = \frac{\rho l}{A} \quad (5.1)$$

gives a resistance $6.8 \text{ k}\Omega$ for a carbon strip of $1000 \times 1000 \times 2 \text{ nm}$, which is a very rough approximation of the effective resistance of the carbon contamination in the gap. This is not strictly valid as the layer thickness is only 2 nm , and ohmic assumptions are not very justifiable at such a small scale.

Deliberately produced thin amorphous carbon films have a wide range of reported resistivities. [62] Films less than 2 nm thick, produced by electron beam induced deposition (EBID) presumable from hydrocarbons in diffusion pump oil, have had resistivities with low bias in the range of $10^9 \text{ }\Omega\text{m}$ according to one source [63]. Carbon interconnects made with EBID from residual hydrocarbons have had a reported resistivity of $0.2 \text{ }\Omega\text{m}$, which has been improved to $5 \times 10^{-3} \text{ }\Omega\text{m}$ with partial graphitization via Joule heating. [64] The latter numbers would mean an original resistance of $100 \text{ M}\Omega$ and $2.5 \text{ M}\Omega$ with heating in the calculated test case. The resistivities for EBID carbon are still orders of magnitude higher than the range of literature values for amorphous carbon and graphite ($(8.5 - 41) \times 10^{-6} \text{ }\Omega\text{m}$), but the ensuing current increase in CNTFETs would be obvious in measurements.

EBID carbon has been used for connecting MWCNTs with metal electrodes, lowering the contact resistance by a claimed two orders of magnitude initially and a similar lowering produced by partial graphitization, the final state corresponding to the resistance of outer shell conduction in the MWCNT. [64]

5.2.1 Effect of an extra Pd layer

Due to poor electrical connections in many samples, an additional 40 nm palladium layer was fabricated on DEP electrode tips after trapping the CNT material for nine samples in batch DEP4. The overall effect of this layer was, against expectations, harmful for the CNTFET devices. An AFM image of the contacts is shown in Fig. 5.7.

A summary of electrical measurements is found in Table 5.2. A large problem with these samples was gate leakage, i.e. an electrical connection with current flow between an electrode on the sample surface and the silicon substrate used as a back gate. For first time trapping on a sample without an additional Pd layer a working FET was produced in 47 out of 350 gaps (13.4 %). Only a subset of gaps, of those that seemed to have at least one CNT connection in SEM micrographs, were electrically measured.

The devices were classified as "Gate leak" if there was an ohmic current leak to the current amplifier when applying a gate voltage and "Working FET" if the device shows a usable semiconducting response with hysteresis. The classification "Other" was used if the device was measured, but the response was something else than the responses mentioned before. These include a metallic response, a semiconducting response without hysteresis or no current response at all.

The data for the same sample with or without an additional Pd layer are not directly comparable, because in many cases measurements were done in more gaps after Pd coating. Almost all of the gaps with FET operation working before the deposition

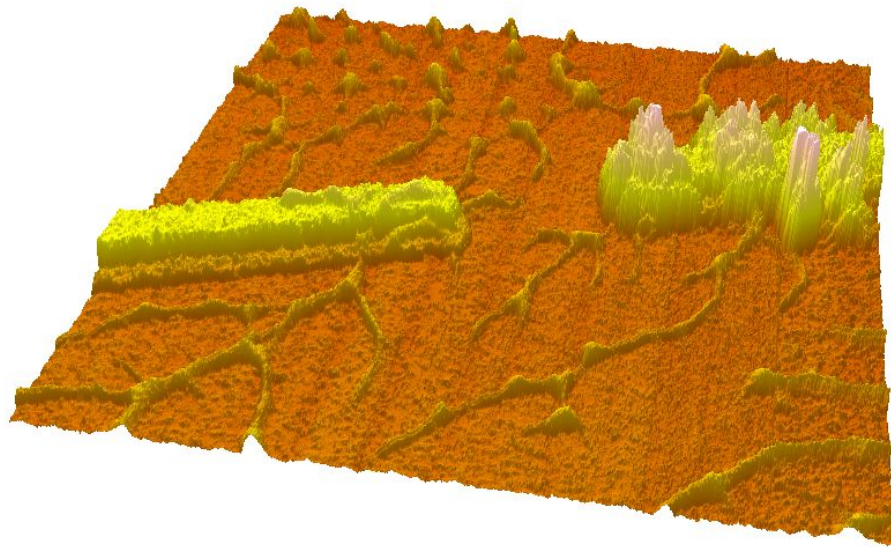


Figure 5.7: An AFM image of a gap used for dielectrophoresis in sample DEP4_13, gap 2. An attempt has been made to produce an additional Pd layer on the existing electrode tips. The gap had two CNTs bridging the gap in SEM imaging and a semiconducting response with a hysteresis effect (on/off ratio 6). The thickness of the electrode on the left is 30 nm and the highest (white) peaks on the right electrode are limited to 70 nm height in the image. The shapes on the substrate are most likely material collected by a liquid (possible water contamination) while drying up.

Table 5.2: The number of working CNT FETs on each sample as well as measured gate leaks and devices without a semiconducting response. Measurements were taken without (left) and with (right) an additional Pd layer.

Sample	Original			Pd top layer		
	Working FET	Gate leak	Other	Working FET	Gate leak	Other
22	4	8	1			
23	6	1	3	5	3	2
24	1	4	2			
6	1	2	4			
12	1	7	2	0	8	2
13	6	1	2	1	12	3
14	7	2	1	5	3	2
8	4	8	4	2	8	5
9	5	4	2	5	5	7
10	4	6	9	2	7	10
11	1	2	4	2	5	9
15	1	1	3			
16	1	4	3			
21	5	6	1			
6r	1	2	4			
15r	2	5	4	1	5	5
Total	50	63	49	23	56	45
With Pd	36	36	31	23	56	45

were remeasured regardless. If the device was not measured after the deposition, the device is marked in Table 5.2 with the same status as before. Therefore only the data for FET operation is strictly comparable when the effect of the Pd layer is considered.

Individual measurements of the width of the hysteresis window and the ratio of currents in on- and off-states are displayed in Tables 5.3 (samples with an additional Pd layer) and 5.4 (no extra Pd layer). The "Device" column shows the sample and gap numbers, while the "Contents" column shows the CNT content of the gap, determined from SEM micrographs. A number in this column tells the number of individual CNTs bridging the gap, "n" is a network of CNTs, "b" is a bundle of CNTs (at least one) and "i" is a larger impurity bridging the gap, usually with a large number of CNTs.

The hysteresis window (first voltage in "Width OFF") is defined as the distance between left and right threshold voltages at the off-state current level. The second voltage is the whole gate voltage sweep, 6 V for all samples in this batch. For example, the gate sweep curve for device DEP4_24_nt22 in Fig. 5.6 gives a hysteresis window of 3 V / 6 V and an on/off ratio of 50 in Table 5.4. The measurement result can also be "leak" because of a current leak to the Si backgate or "-" for other responses, such as a device with no gate response at all or a semiconducting response without a hysteresis window. If the result is empty, no measurements were made.

When considering only gaps that were measured both before and after, the number of working FET devices dropped from 37 to 19 for the samples that received the coating (Table 5.3). Hysteresis windows and on/off ratios did not generally show a significant change in devices that were functional both before and after the processing.

Table 5.3: Electrical measurements, samples without and with (C) a Pd top layer. Explanations for the terms are in the text.

Device	Contents	Width OFF	ON/OFF	C Width OFF	C ON/OFF
23 4	i	0.5V / 6V	1.1	1V / 6V	1.2
23 9	1	1.5V / 6V	1.4	leak	
23 10	1	2V / 6V	2	-	
23 13	i	0.5V / 6V	1.1	0.5V / 6V	1.05
23 16	b	1V / 6V	1.5	1V / 6V	1.2
23 21	1	2V / 6V	2	2.5V / 6V	2
23 23	2	-		1V / 6V	20
12 19	2	1.5V / 6V	1.7	leak	
13 1	4	1V / 6V	1.5	leak	
13 2	2	1.5V / 6V	6	leak	
13 3	1	1V / 6V	1.3	-	
13 11	2	2V / 6V	1.5	leak	
13 17	i	0.5V / 6V	2	leak	
13 18	4	1.5V / 6V	1.2	leak	
13 25	i			1.4V / 6V	1.55
14 1	n	0.5V / 6V	1.4	-	
14 2	n	1.5 V / 6V	2.1	2.0V / 6V	2.04
14 4	4	2V / 6V	1.2	0.5V / 6V	1.2
14 21	n	1V / 6V	1.3	leak	
14 22	n	1.5V / 6V	1.2	1.6V / 6V	1.14
14 23	n	2V / 6V	1.3	1.34V / 6V	1.23
14 24	n	1V / 6V	1.4		
8 2	2	2.5V / 6V	1.4	-	
8 3	5	2V / 6V	1.6	2.5V / 6V	1.3
8 4	3	2V / 6V	2	2V / 6V	1.4
8 19	i	2.5V / 6V	4	-	
9 1	1	2V / 6V	2	1.7V / 6V	1.83
9 2	2	1V / 6V	1.2	-	
9 3	3	1.5V / 6V	5	1.2V / 6V	1.88
9 4	i	-		2.0V / 6V	4.16
9 7	n			0.2V / 6V	1.08
9 9	2	2.5V / 6V	2.3	-	
9 12	3	2V / 6V	1.2	1.5V / 6V	1.18
10 8	3	1.5V / 6V	1.2	1.65V / 6V	1.32
10 9	3	1.5V / 6V	1.3	1.50V / 6V	1.29
10 10	2	0.5 V / 6V	1.2	-	
10 25	i	0.5V / 6V	1.2	leak	
11 3	2	2V / 6V	1.6	1.13V / 6V	1.41
11 17	1			1.41V / 6V	1.87
15r 9	1	2V / 6V	1.2	-	
15r 13	n	2V / 6V	2.3	2V / 6V	1.5

Table 5.4: Electrical measurements, samples without an additional attempt to improve the CNT–electrode interface. Explanations in the text.

Gap	Contents	Width OFF	ON/OFF
22 4	3	1V / 6V	1.5
22 9	b	1.5V / 6V	1.16
22 12	n	1V / 6V	1.13
22 13	n	2V / 6V	2
24 22	4	3V / 6V	50
6r 23	i	2V / 6V	10
15 13	1	2V / 6V	1.6
16 10	i	1.5V / 6V	1.2
21 9	1	1.5V / 6V	1.6
21 16	3	2V / 6V	1.3
21 19	i	2V / 6V	1.2
21 23	1?	1V / 6V	3
21 24	2	1V / 6V	1.2

Chapter 6

Conclusions

6.1 CNT trapping

The yield in trapping a single CNT was 12.5 % for the whole DEP4 batch with 550 electrode gaps evaluated. The electrical parameters used for trapping were the same across all the evaluated samples, with only the CNT concentration varying between samples. However, the amount of attached material on the gaps varied widely even when the concentration was the same as well (Table 5.1). The CNTs were mechanically tightly attached to the substrate after DEP deposition, as sonication and acetone were unable to move them. RIE with oxygen was successful in cleaning samples from CNTs and most impurities.

Individual samples had generally a very wide variety in the amount of CNTs trapped in each gap. This points to inhomogeneity of the DCE suspension, because larger assemblies (particles with diameters in micrometers) of CNTs had often been deposited on the samples during trapping. The bundling and subsequent gathering of CNTs into macroscopic particles was visible even with the bare eye a few hours after sonication.

A big practical problem seems to lie also in controlling the CNT concentration of the applied suspension in addition to its homogeneity. Different samples had a large difference in trapped material even though the suspension was taken from the same bottle at the same time and applied on the samples only minutes apart. However, the samples which had the suspension with the lowest CNT concentration applied to them had the highest average success rate (22 %).

Using surfactants during trapping would homogenize the suspension by preventing bundling and subsequent accumulation into larger particles. This would improve the yield for devices with a single SWCNT. The surfactants could be dissolved away after deposition to ensure a good connection with the electrodes.

Another difficulty in placing the CNTs was the influence of the edges of the electrodes, trapping CNTs uniformly across the electrode structure. Fringing fields from the electrodes to the substrate contribute to this phenomenon, and using a dielectric substrate such as glass might help in directing more CNTs to the gaps themselves. [41]

Producing devices with crossed nanotubes was much more difficult, mostly because the CNTs were deposited on all edges of the electrodes. This meant that adjacent electrodes were most commonly connected rather than opposite ones, even though the opposite electrodes had the DEP voltage applied to them. No functional crossed CNT devices were produced, although some were close as observed with SEM (Fig 5.4).

The most common method in making circuits with CNTs involves spinning the suspension on a surface and locating the tubes with AFM. With AFM images electrodes connecting the tubes are designed and produced with electron beam lithography. This method is more cumbersome than the presented assembly with DEP, but enables the selection of specific tubes for electrical circuits. Spinning the suspension also contaminates the entire surface of the sample with tubes of random distribution and orientation. Direct growing of SWCNTs on an electrode is possible, but this produces catalyst contamination and the selectivity of CNTs is poor.

The yield in produced CNTFETs is acceptable for research applications, but it could be improved using several refinements in the process. If a large CNT density is needed specifically on electrodes, DEP is better than the other methods mentioned.

6.2 FET operation

When considering only the first time DEP was used on a sample, 47 working CNTFETs with hysteresis were produced in 14 samples with 350 electrode gaps, but all of the gaps were not characterized by electrical measurements. There was a problem with gate leakage through the dielectric layer on many (about 40 %, Table 5.2) of the measured devices. The AC DEP voltage used may have been a factor in this, but a test with plain DCE in batch DEP10 suggested that the DEP procedure itself did not damage the gate dielectric noticeably. However, the back gate voltage sweeps were limited to ± 3 V, because higher voltages were found to produce a current leak through the gate for some samples.

A more likely factor is the process of wire bonding. The gate used was the whole silicon substrate (back gate), so the gate dielectric layer could have been damaged under the bonding pads by the combined effect of scratching and ultrasonic excitation by the wire bonder tip. Thicker dielectric layers can be used for a better insulation and using a top gate might also remedy the situation.

The choice of the layered HfO_2 - TiO_2 - HfO_2 gate dielectric was due to a desire to have a consistent hysteresis in V_g - I_{ds} curves [65] [10]. This hysteresis is usable in memory devices, but is a hindrance in normal transistor operation. The sample batch DEP4 had a yield of at least 13.4 % for CNTFETs suitable for memory element research (Table 5.2). This yield can be improved by simply using a larger amount of CNT material, as many devices with a lot of CNTs were functional and a large number of attempts didn't have tubes bridging the gap. However, the electrical contacts between

the tubes and electrodes had very high resistances in most cases.

The ratio between conductances of on- and off-states was generally quite low, with the majority of devices having a ratio below two. This was usually due to the semiconducting channel not closing completely. Reasons for this might include the thin carbon contamination layer deposited in the SEM and the inclusion of metallic tubes in some devices. SEM imaging of the samples was justified even considering the contamination, because the other option for analysing the gaps, AFM, would have been much too time-consuming considering the amount of samples involved. CNTFETs produced outside this work without electron beam exposure across the device have had on/off ratios in the range of thousands (Fig. 1.11).

The Pd coating used in attempt to improve the contact between the electrodes and the CNTs failed to remedy the situation as many FET devices stopped working (Table 5.3), presumably due to the damage sustained in the additional lithography process. In addition to this, the figures of merit for memory devices (hysteresis window and on/off ratio) did not see significant changes due to the extra layer.

Broken electrodes and other disconnections from the voltage sources to the gaps during trapping and measurement were a factor in the poor yield in some devices. The yield in working FETs is further decreased by the inclusion of metallic tubes. The CNT material used in the experiments was made by a non-selective catalytic CVD process, and the tubes were not sorted by their electronic properties. Sorted semiconducting tubes are currently commercially available [6], and using them would remove most of the yield decrease due to this factor.

List of abbreviations

ACEO	alternating current electro-osmotic
AFM	atomic force microscope
ALD	atomic layer deposition
BZ	Brillouin zone
CMOS	complementary metal-oxide-semiconductor
CNT	carbon nanotube
CVD	chemical vapor deposition
DCE	1,2-dichloroethane
DEP	dielectrophoresis
DOS	density of states
EBID	electron beam induced deposition
FET	field-effect transistor
FFF	field-flow fractionation
IPA	isopropyl alcohol
MIBK	methyl isobutyl ketone
MOSFET	metal-oxide-semiconductor field-effect transistor
MWCNT	multi-walled carbon nanotube
PMMA	poly(methyl methacrylate)
RIE	reactive ion etching
SEM	scanning electron microscope
SDBS	sodium dodecylbenzene sulphonate
SWCNT	single-walled carbon nanotube

Bibliography

- [1] Anna-Leena Latvala. The effects of environment on the performance of carbon nanotube memory elements. Master's thesis, Department of Physics, University of Jyväskylä, Jyväskylä, Finland, December 2009.
- [2] M. P. Anantram and F. Léonard. Physics of carbon nanotube electronic devices. *Reports on Progress in Physics*, 69:507–561, March 2006.
- [3] A. Jorio, G. Dresselhaus, and M.S. Dresselhaus. *Carbon nanotubes: Advanced topics in the synthesis, structure, properties and applications*. Springer Verlag, 2008.
- [4] E. T. Thostenson, Z. Ren, and T. W. Chou. Advances in the science and technology of carbon nanotubes and their composites: a review. *Composites Science and Technology*, 61(13):1899–1912, 2001.
- [5] Ville Kotimäki. Carbon nanotube azafullerene peapods and their electronic transport properties. Master's thesis, Department of Physics, University of Jyväskylä, Jyväskylä, Finland, July 2008.
- [6] M.S. Arnold, A.A. Green, J.F. Hulvat, S.I. Stupp, and M.C. Hersam. Sorting carbon nanotubes by electronic structure using density differentiation. *Nature nanotechnology*, 1(1):60–65, 2006.
- [7] P. Delaney, H. Joon Choi, J. Ihm, S.G. Louie, and M.L. Cohen. Broken symmetry and pseudogaps in ropes of carbon nanotubes. *Physical Review B*, 60(11):7899–7904, 1999.
- [8] P. L. McEuen, M. S. Fuhrer, and H. Park. Single-walled carbon nanotube electronics. *IEEE Transactions on Nanotechnology*, 1:78–85, March 2002.
- [9] A. Cresti, N. Nemeç, B. Biel, G. Niebler, F. Triozon, G. Cuniberti, and S. Roche. Charge Transport in Disordered Graphene-Based Low Dimensional Materials. *ArXiv e-prints*, September 2008.
- [10] Marcus Rinkiö. *Carbon nanotube memory devices with high- κ gate dielectrics*. Research report no. 13/2009, Department of Physics, University of Jyväskylä, Jyväskylä, Finland, December 2009.

- [11] J.-C. Charlier, X. Blase, and S. Roche. Electronic and transport properties of nanotubes. *Reviews of Modern Physics*, 79:677–732, April 2007.
- [12] T. Belin and F. Epron. Characterization methods of carbon nanotubes: a review. *Materials Science and Engineering B*, 119(2):105 – 118, 2005.
- [13] Andrew P. Graham, Georg S. Duesberg, Robert V. Seidel, Maik Liebau, Eugen Unger, Werner Pamler, Franz Kreupl, and Wolfgang Hoenlein. Carbon Nanotubes for Microelectronics? *Small*, 1:382–390, February 2005.
- [14] S. Reich, C. Thomsen, and J. Maultzsch. *Carbon nanotubes: basic concepts and physical properties*. Vch Verlagsgesellschaft Mbh, 2004.
- [15] Mahdi Pourfath. *Numerical Study of Quantum Transport in Carbon Nanotube Based Transistors*. PhD thesis, Faculty of Electrical Engineering and Information Technology, Vienna University of Technology, Vienna, Austria, July 2007.
- [16] P. Avouris, Z. Chen, and V. Perebeinos. Carbon-based electronics. *Nature Nanotechnology*, 2:605–615, October 2007.
- [17] Z. Chen, J. Appenzeller, J. Knoch, Y. Lin, and P. Avouris. The Role of Metal-Nanotube Contact in the Performance of Carbon Nanotube Field-Effect Transistors. *Nano Letters*, 5(7):1497–1502, 2005.
- [18] Slava V. Rotkin and Shekhar Subramoney. *Applied physics of carbon nanotubes: fundamentals of theory, optics and transport devices*. Springer, 2005.
- [19] J. Appenzeller, J. Knoch, R. Martel, V. Derycke, S. J. Wind, and P. Avouris. Carbon nanotube electronics. *IEEE Transactions on Nanotechnology*, 1:184–189, December 2002.
- [20] J. Knoch and J. Appenzeller. Tunneling phenomena in carbon nanotube field-effect transistors. *physica status solidi (a)*, 205(4):679–694, November 2008.
- [21] J. P. Sun, Z. X. Zhang, S. M. Hou, G. M. Zhang, Z. N. Gu, X. Y. Zhao, W. M. Liu, and Z. Q. Xue. Work function of single-walled carbon nanotubes determined by field emission microscopy. *Applied Physics A: Materials Science & Processing*, 75:479–483, 2002.
- [22] A. Star. Nanotube optoelectronic memory devices, June 8 2005. US Patent App. 11/147,535.
- [23] V. Derycke, R. Martel, J. Appenzeller, and P. Avouris. Carbon nanotube inter-and intramolecular logic gates. *Nano Letters*, 1(9):453–456, 2001.

- [24] W. Lu and C. M. Lieber. Nanoelectronics from the bottom up. *Nature Materials*, 6:841–850, November 2007.
- [25] M. S. Fuhrer, B. M. Kim, T. Dürkop, and T. Brintlinger. High-Mobility Nanotube Transistor Memory. *Nano Letters*, 2:755–759, July 2002.
- [26] M. Rinkiö, A. Johansson, M. Y. Zavodchikova, J. Jussi Toppari, A. G. Nasibulin, E. I. Kauppinen, and P. Törmä. High-yield of memory elements from carbon nanotube field-effect transistors with atomic layer deposited gate dielectric. *New Journal of Physics*, 10(10):103019–+, October 2008.
- [27] Kimmo Laitinen. Fluid dynamics in DEP trapping of DNA origamis and their functionalization. Master’s thesis, Department of Physics, University of Jyväskylä, Jyväskylä, Finland, April 2009.
- [28] Tommi Hakala. *Applications of light-matter interaction in nanosciences*. Research report no. 14/2009, Department of Physics, University of Jyväskylä, Jyväskylä, Finland, December 2009.
- [29] Sampo Tuukkanen. *Dielectrophoresis as a tool for on-chip positioning of DNA and electrical characterization of nanoscale DNA*. Research report no. 13/2006, Department of Physics, University of Jyväskylä, Jyväskylä, Finland, December 2006.
- [30] J. Li, Q. Zhang, D. Yang, and J. Tian. Fabrication of carbon nanotube field effect transistors by AC dielectrophoresis method. *Carbon*, 42(11):2263–2267, June 2004.
- [31] T. B. Jones. Basic theory of dielectrophoresis and electrorotation. *Engineering in Medicine and Biology Magazine, IEEE*, 22:33–42, November 2003.
- [32] M. Pycraft Hughes. AC electrokinetics: applications for nanotechnology. *Nanotechnology*, 11:124–132, June 2000.
- [33] Veikko Linko. Dielectrophoresis of thiol-modified origami. Master’s thesis, Department of Physics, University of Jyväskylä, Jyväskylä, Finland, December 2007.
- [34] Michael P. Hughes. *Nanoelectromechanics in engineering and biology*. CRC Press, 2002.
- [35] Frank M. White. *Fluid Mechanics, 6th Edition*. McGraw-Hill, New York, USA, 2008.
- [36] N. G. Green, A. Ramos, A. Gonzalez, H. Morgan, and A. Castellanos. Fluid flow induced by nonuniform ac electric fields in electrolytes on microelectrodes. I. Experimental measurements. *Physical Review E*, 61(4):4011–4018, 2000.

- [37] P.R.C. Gascoyne and J. Vykokoukal. Particle separation by dielectrophoresis. *Electrophoresis*, 23:1973–1983, 2002.
- [38] P. J. Burke. Nanodielectrophoresis: Electronic Nanotweezers. *Encyclopedia of Nanoscience and Nanotechnology*, 6(1):623–641, 2004.
- [39] A. Kuzyk, B. Yurke, J. J. Toppari, V. Linko, and P. Törmä. Dielectrophoretic Trapping of DNA Origami. *Small*, 4:447–450, March 2008.
- [40] T. K. Hakala, V. Linko, A.-P. Eskelinen, J. J. Toppari, A. Kuzyk, and P. Törmä. Field-Induced Nanolithography for High-Throughput Pattern Transfer. *Small*, 5:2683–2686, October 2009.
- [41] S. Sorgenfrei, I. Meric, S. Banerjee, A. Akey, S. Rosenblatt, I. P. Herman, and K. L. Shepard. Controlled dielectrophoretic assembly of carbon nanotubes using real-time electrical detection. *Applied Physics Letters*, 94:053105, 2009.
- [42] J. Li, Q. Zhang, N. Peng, and Q. Zhu. Manipulation of carbon nanotubes using AC dielectrophoresis. *Applied Physics Letters*, 86(15):153116–+, April 2005.
- [43] M. Oron-Carl, F. Hennrich, M. M. Kappes, H. V. Löhneysen, and R. Krupke. On the Electron-Phonon Coupling of Individual Single-Walled Carbon Nanotubes. *Nano Letters*, 5:1761–1767, September 2005.
- [44] N. Chimot, V. Derycke, M. F. Goffman, J. P. Bourgoin, H. Happy, and G. Dambrine. Gigahertz frequency flexible carbon nanotube transistors. *Applied Physics Letters*, 91(15):153111–+, October 2007.
- [45] P. G. Collins, M. S. Arnold, and P. Avouris. Engineering Carbon Nanotubes and Nanotube Circuits Using Electrical Breakdown. *Science*, 292:706–709, April 2001.
- [46] P. Stokes and S. I. Khondaker. Local-gated single-walled carbon nanotube field effect transistors assembled by AC dielectrophoresis. *Nanotechnology*, 19(17):175202–+, April 2008.
- [47] T. Schwamb, T.-Y. Choi, N. Schirmer, N. R. Bieri, B. Burg, J. Tharian, U. Sennhauser, and D. Poulidakos. A Dielectrophoretic Method for High Yield Deposition of Suspended, Individual Carbon Nanotubes with Four-Point Electrode Contact. *Nano Letters*, 7:3633–3638, December 2007.
- [48] A. Hasan, A. Pal, and A. Ghatak. Dielectric Relaxation of 1, 2-Dichloroethane and 1, 2-Dibromoethane in the Liquid State. *Bulletin of the Chemical Society of Japan*, 44(2):322–324, 1971.
- [49] M. Dimaki and P. Bøggild. Dielectrophoresis of carbon nanotubes using micro-electrodes: a numerical study. *Nanotechnology*, 15:1095–1102, August 2004.

- [50] Marina Zavodchikova. Memory effects in carbon nanotube-based transistors and ways towards their controlled fabrication. Master's thesis, Department of Physics, University of Jyväskylä, Jyväskylä, Finland, May 2007.
- [51] R. Krupke, F. Hennrich, H. v. Löhneysen, and M. M. Kappes. Separation of Metallic from Semiconducting Single-Walled Carbon Nanotubes. *Science*, 301:344–347, July 2003.
- [52] K. W. C. Lai and N. Xi. Novel Carbon Nanotube Deposition System for Fabricating Nano Devices. In *2nd IEEE International Conference on Nano/Micro Engineered and Molecular Systems, 2007. NEMS'07*, pages 1081–1084, 2007.
- [53] R. Krupke, F. Hennrich, M. M. Kappes, and H. v. Löhneysen. Surface Conductance Induced Dielectrophoresis of Semiconducting Single-Walled Carbon Nanotubes. *Nano Letters*, 4:1395–1399, August 2004.
- [54] S. Banerjee, B. E. White, L. Huang, B. J. Rego, S. O'Brien, and I. P. Herman. Precise positioning of single-walled carbon nanotubes by ac dielectrophoresis. *Journal of Vacuum Science Technology B: Microelectronics and Nanometer Structures*, 24:3173–+, 2006.
- [55] M. Ouyang, M. L. Y. Sin, G. C. T. Chow, W. J. Li, X. Han, and D. C. Janzen. DEP-based fabrication and characterization of electronic-grade CNTs for nano-sensing applications. In *7th IEEE Conference on Nanotechnology, 2007. IEEE-NANO 2007*, pages 1–6, 2007.
- [56] M. Y. Zavodchikova, A. Johansson, M. Rinkiö, J. J. Toppari, A. G. Nasibulin, E. I. Kauppinen, and P. Törmä. Fabrication of carbon nanotube-based field-effect transistors for studies of their memory effects. *physica status solidi (b)*, 244:4188–4192, August 2007.
- [57] M. Rinkiö, M. Y. Zavodchikova, P. Törmä, and A. Johansson. Effect of humidity on the hysteresis of single walled carbon nanotube field-effect transistors. *physica status solidi (b)*, 245:2315–2318, June 2008.
- [58] A. Vladar and M. Postek. Electron beam-induced sample contamination in the sem. *Microscopy and Microanalysis*, 11(Supplement):764–765, 2005.
- [59] M.T. Postek. An approach to the reduction of hydrocarbon contamination in the scanning electron microscope. *Scanning*, 18(4):269–274, 1996.
- [60] MAOL ry. *MAOL-taulukot*. Kustannusosakeyhtiö Otava, Keuruu, 1996.
- [61] Hugh D. Young and Roger A. Freedman. *University Physics with Modern Physics, 11th Edition*. Pearson Education Inc., San Francisco, USA, 2004.

- [62] A. Reznik, V. Richter, and R. Kalish. Kinetics of the conversion of broken diamond (sp^3) bonds to graphitic (sp^2) bonds. *Physical Review B*, 56(13):7930–7934, 1997.
- [63] N. Miura, H. Ishii, J. Shirakashi, A. Yamada, and M. Konagai. Electron-beam-induced deposition of carbonaceous microstructures using scanning electron microscopy. *Applied Surface Science*, 113:269–273, 1997.
- [64] Konrad Rykaczewski. *Electron beam induced deposition (EBID) of carbon interface between carbon nanotube interconnect and metal electrode*. PhD thesis, Georgia Institute of Technology, Atlanta, GA, USA, November 2009.
- [65] Marcus Rinkiö, Andreas Johansson, G. S. Paraoanu, and Päivi Törmä. High-Speed Memory from Carbon Nanotube Field-Effect Transistors with High- κ Gate Dielectric. *Nano Letters*, 9(2):643–647, February 2009.